

Fluidic Computation Kit: Towards Electronic-free Shape-changing Interfaces

Qiuyu Lu
Carnegie Mellon University
Pittsburgh, PA, USA
qiuyul@cs.cmu.edu

Haiqing Xu
Tsinghua University
Beijing, China
xhq20@mails.tsinghua.edu.cn

Yijie Guo
Tsinghua University
Beijing, China
gyj21@mails.tsinghua.edu.cn

Joey Yu Wang
Carnegie Mellon University
Pittsburgh, PA, USA
jywang@cs.cmu.edu

Lining Yao
Carnegie Mellon University
Pittsburgh, PA, USA
liningy@cs.cmu.edu

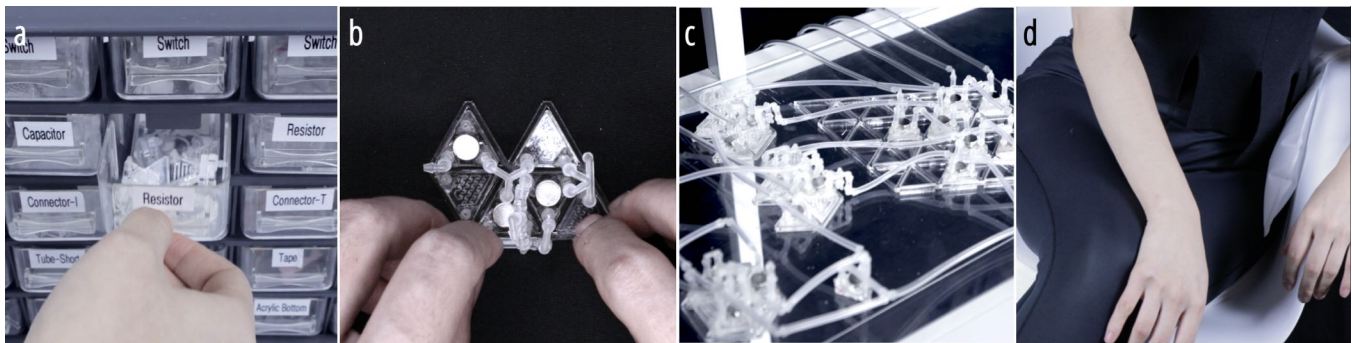


Figure 1: Building interface with embedded mechanical computations enabled by Fluidic Computation Kit. a) Pick the elementary pieces from the component library. b) Construct an operator (register) via wiring the components. c) A parallel processor is achieved by combining different operators. d) A fluidic computation augmented chair that can monitor different sitting positions and alert the user when a poor posture is detected.

ABSTRACT

Although fluidic computation has been utilized to develop interactive devices in the field of Human-Computer Interaction (HCI), the limited computation complexity of previous work hinders the exploration of richer interaction modalities. Based on the Fluidic Computation Kit we developed, this paper explores how unconventional mechanical computing can be leveraged to design shape-changing interfaces that integrate input sensing, output, and complex computation. After introducing the design space enabled by the Kit, we explain how to design four types of elementary computational components and six categories of operators. We end by providing several application scenarios which illustrate the Fluidic Computation Kit's potential to build sophisticated circuits (e.g., a parallel processor) for use in the field of HCI.

CCS CONCEPTS

• **Human-centered computing** → **Interactive systems and tools.**

KEYWORDS

shape-changing interfaces, mechanical computation, logic, pneumatic, fabrication

ACM Reference Format:

Qiuyu Lu, Haiqing Xu, Yijie Guo, Joey Yu Wang, and Lining Yao. 2023. Fluidic Computation Kit: Towards Electronic-free Shape-changing Interfaces. In *Proceedings of the 2023 CHI Conference on Human Factors in Computing Systems (CHI '23)*, April 23–28, 2023, Hamburg, Germany. ACM, New York, NY, USA, 21 pages. <https://doi.org/10.1145/3544548.3580783>

1 INTRODUCTION

The advancement of technology in the information age has led to a shift from mechanical to electronic computation forms [3, 17]. In Human-Computer Interaction (HCI), embedded electronic chips are now widely used as the computational units for prototyping physical computing interfaces and devices. However, there is a recent trend towards the development of unconventional forms of computation that incorporate cutting-edge engineering knowledge and manufacturing capabilities, such as robotics, informational processing, and materials science [63]. Although unconventional



This work is licensed under a Creative Commons Attribution-NonCommercial-ShareAlike International 4.0 License.

CHI '23, April 23–28, 2023, Hamburg, Germany
© 2023 Copyright held by the owner/author(s).
ACM ISBN 978-1-4503-9421-5/23/04.
<https://doi.org/10.1145/3544548.3580783>

computation has found success in several science and engineering applications, including molecular computation [1], robotics [42, 59], morphological computation [22], and fluidic logic circuits [35, 45, 64], its adoption within the HCI device fabrication and design community is still in its early stages, with only a few recent pioneering works [10, 25, 34, 47].

Building on top of existing literature, here we use fluidic computation as an example to further explore how complex unconventional mechanical computing can be leveraged by HCI researchers and designers, or even the public (Fig. 1). In particular, we identified the following unique gap to address: there is a lack of elementary toolkit or library for prototyping powerful fluidic computation circuits yet:

To understand electronic circuits, we must first study the basic laws and the elementary components in electronics. Moreover, with various electronic components available, we can conveniently build, customize or upgrade circuits with different functions. Microfluidic chips are generally known to be highly integrated, just like the electronic integrated circuits [35, 45, 64]. Previous work in the field of robotics have deconstructed microfluidic chips a little by designing complex pneumatic structures with multiple ports that can operate as one kind of logic gates at a time, just like electronic logic chips with many pins [8, 41]. While these (micro)fluidic devices are like black boxes, several recent works [12, 28, 40, 43] focused on pushing the design of the single valve (switch) and building fluidic circuits with them. However, the lack of further design on other elementary fluidic components beyond the switch limited the types of circuits that users can explore and build. By pursuing this trend, we aim to offer a fundamental, reconfigurable, and user-friendly approach to learning and constructing a variety of fluidic computation devices.

To address the gap above, this paper will present the Fluidic Computation Kit that breaks down fluidic computation devices and provides a relatively rich set of building library. Interfaces that have fluidic logic fully analogous to electronic logic with significant complexity advances over the previous implementations shown in HCI literature [10, 34, 47] can be built with the Kit. We also derive a design space to couple extended I/O modalities in the design of fluidic computation integrated interfaces, and demonstrate HCI-relevant applications to emphasize the electronic-free, I/O coupling and learning & play aspects. We hope our Kit can potentially make fluidic computation devices more accessible and disseminate related knowledge and concept.

The core contributions of this work are as follows:

- The Fluidic Computation Kit that provides a richer set of library for prototyping fluidic computation devices. It covers all the way from multiple elementary components to various high-level operators.
- Four types of elementary components are designed. Beyond the switch; the diode, a range of resistors in different values, and capacitors with various functionalities are also introduced;
- Six categories of computational operators (i.e., logic gates, filter, timer, register, edge detector, and (de)multiplexer) enabled by simply wiring the aforementioned computational components are explored, including the novel passive filter and timer operator;
- The design space of complex fluidic computation embedded shape-changing interface;
- Characterization for the fluidic computation components and operators;
- Several application scenarios, demonstrating the Fluidic Computation Kit's ability to build complex circuits (e.g., parallel processor) and the potential of adopting the fluidic computation in HCI.

2 RELATED WORK

2.1 Fluid-driven Interfaces

Fluid-driven interfaces have been extensively investigated in HCI. In past decades, an abundance of work has contributed to greatly expanding such interfaces' fabrication materials and methods, shape-changing capabilities, and actuation structures [15, 32, 33, 37, 46, 60–62]. Actuation methods beyond bulky compressors and pumps have been investigated [18, 32, 58]. Sensing technologies utilizing fluid-driven interfaces have also been studied [23, 51].

Leveraging the technical advances of the fluid-driven interface, various studies regarding application context exploration and user experience evaluation have emerged. Many of them investigate various haptic feedback experiences enabled by fluid-driven interfaces, such as Force Jacket [9], HydroRing [20], PuPoP [52], Chemical Haptics [31], etc. Moreover, there has also been exploration in using fluid-driven interfaces as a pleasant, aesthetic display [50], or even enhancing people's creativity [30].

From fabrication, sensing, actuation, to application, fluid-driven interfaces thrive comprehensively except for one aspect - computing. Most fluid-driven interfaces are still controlled by bulky valves and electronic control boards.

2.2 Integrating Mechanical Computation to Interface

Recently, we have seen a trend of pushing computing power further by adopting unconventional forms of computation. A few studies in HCI have tried to integrate mechanical computation into the interface. Venous Materials [34] demonstrates fluidic mechanisms that can respond to a user's mechanical inputs and display an output. However, it can only visually display, and the "computation" is limited to mapping the force with how far liquid can be squeezed. Logic bonbon [10], based on "beam deflection" mechanism [44], builds some basic logic gates that can be used to make desserts with different flavor combinations based on the user's input.

AirLogic [47] pushes such basic mechanical logic gates further by integrating it into a 3D printing process and augmenting it with various input and output widgets. However, such a "beam deflection" mechanism is limited in its computational capabilities. It can only achieve several basic logic gate structures and such gates do not have a good cascaded ability, which prevents them from composing complex circuits with various mechanical computation abilities. Moreover, the output airflow from a logic gate based on "beam deflection" mechanism is hard to be used to actuate the inflatables. Such a logic gate structure usually has multiple outlets connected to the atmosphere, only one of which is considered an output channel. When the airflow of inputs does not travel to the output under the action of the "beam deflection" mechanism, it

needs to be excluded from other outlets. This means that when we connect an airbag to the output, even though the output should be 1, the airbag cannot be effectively pressurized. Because the air will flow out from the other outlets connected to the atmosphere, the logical operation is disturbed. This is an inherent limit of the mechanism: pressure building up too much at the output port will interfere with its logic operation. This limitation greatly prevented such fluidic-logic structures from integrating with the previous pneumatically-driven shape changing output techniques from literature, resulting in limited application contexts.

Beyond fluid-driven computation, Ion et al. introduced digital mechanical metamaterials that can be used to build logic structures [25]. However, circuits built with such metamaterials require a manual reset after each use to recover the lost energy.

2.3 (Micro)fluidic Computation

In the past few decades, (micro)fluidic computation has received growing interest. (Micro)fluidic computational technology has developed from basic logic gates enabled by beam reflection mechanism [44] to more complex fluidic switch (valve), resistor, capacitor, and higher level computational operators [35, 45, 64]. The fluidic switch, which is usually called a Quake valve [54, 55], has a two-layer structure, with a target channel and a control channel on each layer. The target channel can be blocked or unblocked by tuning the deformation of an elastic membrane through air pressure change in the control channel. Computational structures with various functions including logic gates [2], filter [29], d-latch [45], oscillator [13], and multiplexer [54] have been built in this way. However, these computational structures are vacuum-atmosphere based. The fluid is drained out of the system rather than pumped into the system. Since human actions are typically more easily converted into positive air pressure changes [14, 27, 34], the vacuum-atmosphere-based computational structure is not ideal for a fluid-driven interface design that involves human input.

Though rare, a few studies explored positive air pressure actuated microfluidic computation structures [11, 19, 57]. They share the principle that the valve must have a static gain property that allows the target channel to get blocked even when the air pressure in the control channel is relatively low. However, their static gain switch is more complex than the standard microfluidic valve and is much harder to fabricate. Furthermore, it has not been verified whether such a switch design can still operate after being scaled up and working at a higher pressure which actuating “macro” interaction devices would need.

Beyond the microfluidic field, fluidic computation has also been widely adopted for robot design. Some works focus on using a high-end 3D printer to fabricate integrated fluidic circuits in a single print run [24, 59]. In contrast, some works deconstructed the highly integrated fluidic circuits a little by designing novel modular pneumatic structures [8, 41]. Such modules usually have multiple input ports. Furthermore, by selectively using some of the ports, the module can work as Gate NOT, AND, OR, etc., acting like the small electronic logic chips have many pins with different functions. Such modules are still like black boxes to the user.

Recently, several works [12, 28, 40, 43] focus on improving the single valve (switch) design and building fluidic circuits with it.

Rajappan et al. [43] demonstrated fluidic operators built with heat-sealed textile switches, like basic logic gates, SR latch, etc. However, the lack of other basic fluidic computation components in this work impairs the potential of building more kinds of operators like filters and timers introduced in our Kit. Drotman et al. [12] and Preston et al. [40] built ring oscillators based on a silicone-casted bistable valve that they called 3/2 soft valves. And they used thin tubings as resistors and glass jars as capacitors to regulate the oscillation. However, for most users, it may be difficult for them to obtain the desired resistance value by adjusting the length, thickness, or even the material of the tubing; the characteristics of a “glass jar capacitor” can also be a mystery. In short, while focusing on switches, how other components, such as the resistors and capacitors, can be isolated, designed, and evaluated are much less studied.

In comparison, we have designed a Fluidic Computation Kit that breaks down fluidic computation and provides a rich set of elementary components as well as functional operators library for learning and prototyping fluidic computation circuits, both simple and complex. In addition to the switch, we also introduce the diode, the resistors with clearly specified resistances, and the capacitors with various properties that have not been widely discussed in the literature. By combining these components, the Kit enables the creation of novel operators and complex circuits.

3 DESIGN SPACE

The fluidic computational interface integrates force input, computation, and tangible output, relying on mechanical structures. We believe such electronic-free interfaces are capable of coupling various kinds of I/O when designing physical and material-based interfaces. We share a diagram described in Fig. 2 to map out the design space:

Input: Designing the input modalities/devices has been an critical aspect of interface design [5]. Many human behaviors involve force changes. And when such force changes are applied to airbags, they induce air flow/pressure change. Here we focus on leveraging the simple airbags as transducers from the physical properties of the world [4] into the fluidic circuits. We define eight major types of force change inputs that can be detected with the fluidic circuits built with our Kit.

- **Magnitude:** The force magnitude change can cause an airbag’s inner air pressure to change. The fluidic switch in the Kit has a tunable burst pressure threshold, which can be leveraged to detect different force magnitudes.
- **Duration.** A continuous force will lead to an air pressure change last for a certain time. The fluidic timer can be used to monitor the duration of such a force.
- **Frequency:** The periodic force change can be converted to periodic air pressure change. The fluidic filter can process such force changes and regulate its output air flow rate based on the frequency.
- **Impulse.** The sudden force change will result in a rising or falling edge of air pressure. The fluidic edge detector is designed to monitor such a force impulse.
- **Distribution:** Multiple airbags can be used to detect the force distribution at desired points. Many fluidic operators (e.g.,

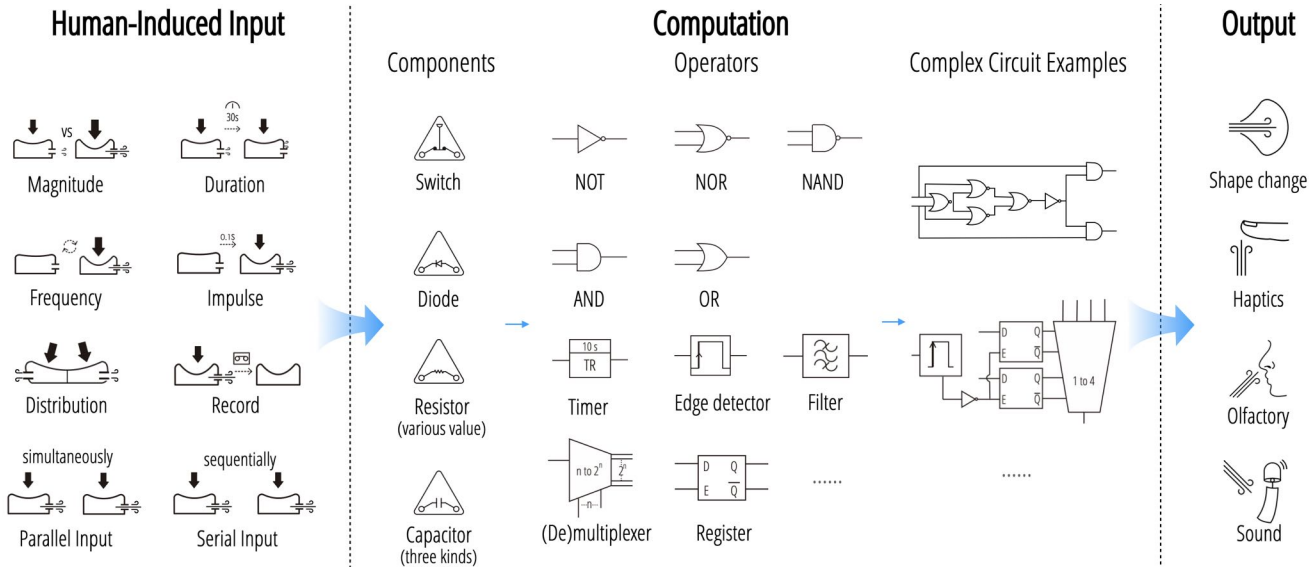


Figure 2: Design space of fluidic computational interface enabled by our Kit. Human actions can induce forces, which can be converted into air pressures as *input* for the *computational* units. Then, the fluidic computational unit generates fluidic-driven *output* that results in proper responses to the users.

the demultiplexer) and circuits that can process multiple input air pressure signals can be leveraged to monitor the force distribution.

- **Record:** The fluidic register can be used to store the force change history.
- **Parallel Input:** As mentioned above, fluidic operators or circuits (e.g., a parallel processor) can be built to monitor several force inputs simultaneously.
- **Serial Input.** Theoretically, a shift register [45] can be built with the Kit, enabling continuous monitoring of the change of a force input over time.

Computation: Input force(s) converted into the airflow will then become the input signal(s) of the fluidic computational circuits, which compute and generate the fluid-driven tangible output(s). The basic functions of several fluidic operators and circuits have been briefly discussed above. The detailed mechanism and operation will be introduced in the following section.

Output: The computation results are delivered in the form of airflow which can be leveraged in pneumatically-driven shape-changing interfaces for interaction or information display. Four output modalities can be achieved, including shape change, airflow-induced haptics, olfactory response (e.g., infusing essential oil into the airflow to wake someone from sleeping), and acoustic feedback (e.g., whistling through the airflow).

4 FLUIDIC COMPUTATION KIT

4.1 Overview

Our Kit includes basic computational components (i.e., switch, diode, resistor, and capacitor) and operators (logical gates, filter, timer, register, edge detector, and (de)multiplexer). In terms of their

form factor, we chose a triangle shape that 1) best matches the functional structure of the most frequently used switch component, and 2) can make the assembly and layout of components more compact, flexible, and aesthetically pleasing.

Before diving into the Kit, we clarify the basic analogy between fluidic systems and electrical systems. In electrical circuits, the voltage and current describe the magnitude of the effort and the flow. In a fluidic system, The effort is pressure, and flow is volumetric flow rate [38, 48]. Therefore, we can map these terms as below:

- Power source = Positive pressure air supply (P. Sup.)
- Ground = Atmosphere (ATM)
- High voltage signal = Positive pressure signal (1)
- Zero voltage signal = Atmospheric pressure signal (0)

Since ATM is defined as ground, all air pressure values presented in this paper are gauge pressure built on standard atmospheric pressure.

4.2 Basic Computational Components

Our basic components include the switch (static gain, normally-connected valve), the diodes (one-way valve), the resistor (long, narrow, circuitous channel), and the capacitor (large, deformable chamber) (Table 1). The supportive accessories (the mounting frames, the connectors, and the water tub) are also briefly described here.

4.2.1 Switch - Static Gain Normally Connected Valve. The switch Fig. 3 is the most frequently used building block. The core functional part of the switch consists of an upper target channel that the bottom control channel can block. Fig. 3a, b demonstrates how a switch component works. Its target channel inlet is connected to a positive pressure source, its outlet is connected to a triangular water tub, and its control channel is connected to an airbag. When the airbag is pressed, air pressure in the control channel builds up,

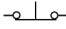

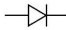

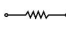

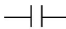

Components	Conventional Electrical Diagram	Fluidic Computational Kit Diagram	Function
Switch			Static gain normally connected valve, blocked when the control channel pressure reaches the threshold.
Diode			One-way valve, allows only unidirectional flow of fluid.
Resistor			Long narrow circuitous channels, can reduce the flow rate, pull up pressure, etc.
Capacitor			Adaptor and Large deformable chamber, versatile components that can work as a buffer, power storage, power supply, etc

Table 1: Summary of the basic components in the Fluidic Computational Kit

causing the target channel to be blocked. In our media, this can be visualized with the demonstrative triangular water tub, which is not used in actual applications. When air exits the outlet, bubbles are visible in the tub. When the target channel is sealed, bubbles are not visible.

The switch (Fig. 3) is one of the most frequently used components, and its structure is also the most complex among our components. The major functional parts include two air channels vertically stacked to each other (target and control channel), one magnetic disk on top of each air channel (top and bottom magnet), and an elastic membrane in the middle. When the positive air pressure builds up in the control channel, the membrane will rebound, and the bottom magnetic will bond with the top magnet and block the target channel. Due to the magnets, relatively small air pressure fluctuation in either channel will not change the current state of the switch. Suppose the control channel pressure builds up and eventually becomes larger than the sum of the target channel pressure and magnetic attraction force. In that case, the control channel will unblock itself to push the bottom magnet downwards and block the control channel. As a result, the switch component switched its state.

To build complicated circuits, cascade ability is critical. Fig. 3c demonstrates that the preceding switch’s output signal (from the target channel) is fed to the control channel of the successive switch. The pressure will drop as air travels through the channels. So, to achieve a fully functional switch with cascade, we must design a valve in which the target channel can be blocked even when the control channel has a lower air pressure than the target channel. Moreover, we need to keep the flow resistance of the switch low to minimize air pressure loss. After testing more than 30 designs, we

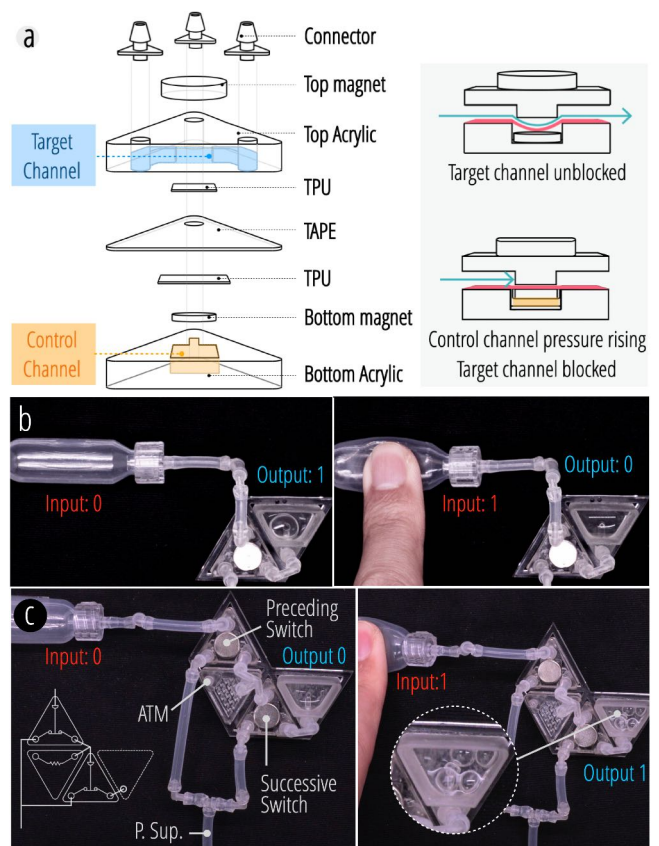


Figure 3: The fluidic switch. a) Exploded views of the switch and the working mechanism. b) The switch works in single. c) Two switches in cascaded connection.

settled on the current static-gain normally connected valve, which leverages magnetic force (Fig. 3.a) and has low flow resistance. Due to the magnets’ existence, the target channel’s air pressure must reach 10 kPa (bursting pressure) to burst through. Moreover, 10 kPa is defined as the baseline in our system that can be considered as 1. A series of experiments are carried out to validate the design, and they are discussed in the later Performance section.

Lastly, as shown in Fig. 3.c, an intervening vent is reserved at the connection point between the two switches. Otherwise, the output from the preceding switch will not be able to restore to atmospheric pressure (0) properly. Because once its target channel gets blocked, air will be trapped at the control channel of the successive switch. Meanwhile, a pull-up resistor before the vent is also required to ensure the pressure can properly build up when the preceding switch gate outputs 1. The same principle usually goes for chaining operators to build advanced circuits, and needs to be kept in mind.

4.2.2 Diodes - One-way Valve. The diode (Fig. 4) is a check valve, which only allows fluid to flow in one direction. As is shown in Fig. 4.a, the diode has the same upper layer structure as the switch. However, instead of having a control layer, the diode has a small rectangle chamber in the bottom layer. Illustrated in Fig. 4.b, when the fluid travels from the left to right side, the fluid will

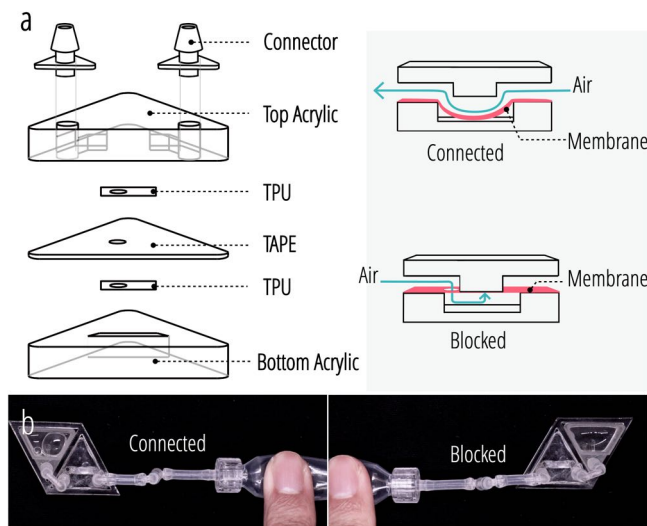


Figure 4: The fluidic diode. a) Exploded views of the diodes and the working mechanism b) Functional prototype of the check valve. Air can pass through the valve from the right side but cannot from the left side.

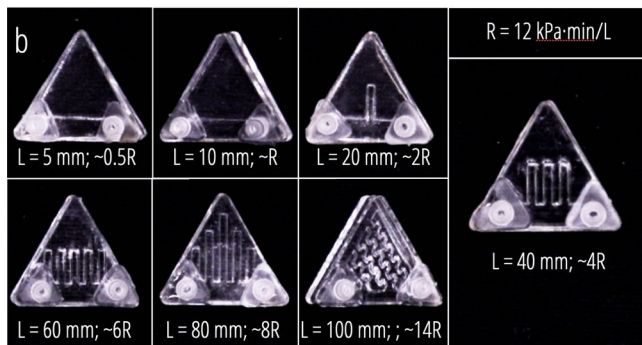
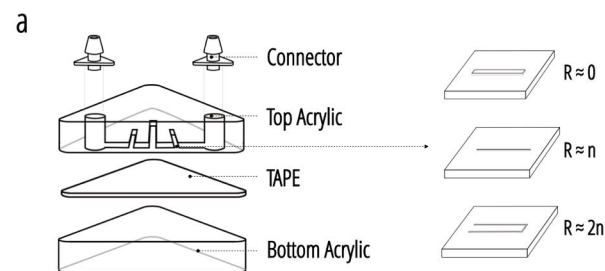


Figure 5: The fluidic resistors. a) Exploded views of the resistor and the mechanism. b) Different lengths of the resistor with folded narrow channels.

flow to the bottom layer chamber through the small hole on the elastic membrane, get trapped, build up pressure, then push the membrane strongly against the upper layer. Thus, it will stop itself from traveling to the right outlet. On the contrary, pressure cannot

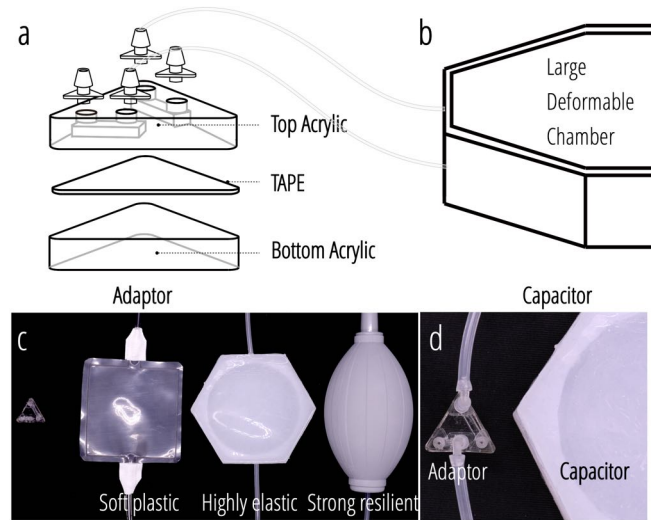


Figure 6: The fluidic capacitors. a) Exploded views of the triangle adaptor. b) Deformable chamber as a fluidic capacitor. c) Three kinds of capacitor prototypes with unique functions. d) Connection method of capacitors and the triangle adaptor.

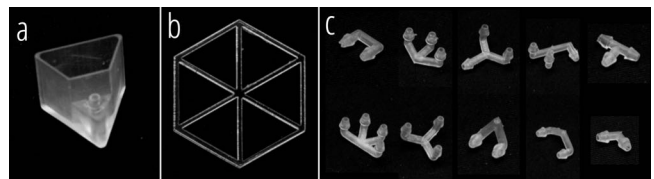


Figure 7: The accessories. a) the water tub for air flow monitoring when testing. b,c) the connectors and one of the frames used for wiring.

build up when fluid travels in the opposite direction as there is an open end (the left outlet).

4.2.3 Resistor - Long Narrow Circuitous Channel. The resistors are components with various long, narrow, circuitous channels with high flow resistance (Fig. 5.a). They can reduce the flow rate, pull up the pressure, etc. They come with various resistances, and users can choose or combine them to get desired values.

The resistance is generally linear to the channel length for straight thin channels with the same cross-section geometry (Fig. 5.b). Since the resistor components are very compact, we must fold the narrow channel up to 100 mm in length and 1 mm in gap width to fit. We carried out an experiment to measure the resistance, and the result confirmed that it changes linearly to the length. The detailed result is presented in the later Performance section.

4.2.4 Capacitor - Large Deformable Chamber. The capacitor is a very versatile component and plays a critical role in many operators. It consists of a triangle adaptor (Fig. 6.a) and a relatively large deformable chamber (Fig. 6.b). Various kinds of chambers can be adopted for the capacitor components to achieve different functions (Fig. 6.c). For example,

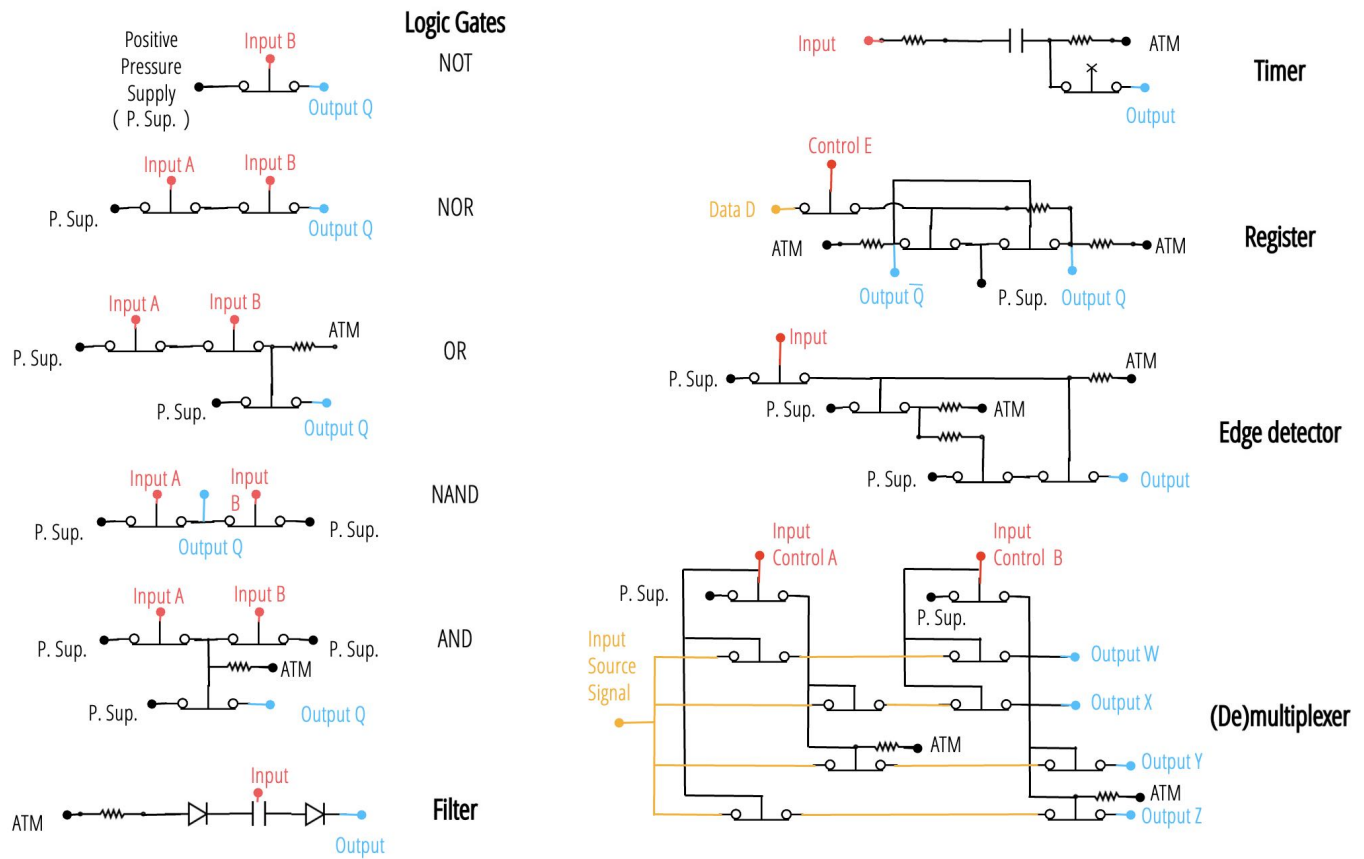


Figure 8: The wiring diagram which discards the form factor of all the operators.

- (1) a thin, soft, (prefold) plastic air bag is suitable to work as a buffer as it is easy to get inflated and can store lots of air before pressure builds up;
- (2) a highly elastic (silicon) chamber can perform as energy storage since once it is charged and gotten inflated, it will actively deflate and continually power the circuit for a while after the air source stops;
- (3) a strong resilience chamber can restore energy automatically after being squeezed. When operated with periodic external force, such a capacitor can work as a pump.

4.2.5 *Accessories.* To facilitate the wiring process, we designed cellular frames for fixing the components (Fig. 7.a), and various connectors for connecting components in different numbers and orientations (Fig. 7.b). To intuitively visualize the output when testing the components and operators, a triangle water tub which has the same dimension as the components is designed (Fig. 7.c).

4.3 Computational operators

Various types of operator can be constructed with aforementioned components. In this subsection, we will discuss six types of example operators we build, including logic gates, filter, timer, register, edge detector, and (de)multiplexer. The wiring diagram which discards the form factor is as Fig. 8.

4.3.1 *Logic gates.* A logic gate is the operator that can implement a Boolean function. It can take one or more high (1) or ATM(0) pressure airflow inputs either directly from the user or from the preceding circuit, then perform the logic operation, and output positive pressure air flow (1) or nothing (0). Logic gates can be implemented primarily using the switch components. Here we describe the design and operation of five logic gates:

NOT. Not gate, also known as the inverter, can invert the input, which means outputs 1 (positive pressure) if the input is 0 (ATM). A single switch component can work as a NOT gate (Fig. 3.b). Though simple, NOT gate is one of the most frequently used operators when building advanced fluidic circuits, as inverting preceding circuit output is often necessary.

NOR, NAND. NOR gate (Fig. 9.a) is constructed with two serial switches, which means only when both switches are open (both inputs are 0), air from the positive pressure source will flow through the target channel and generate a positive pressure output (1). Similarly, the NAND gate (Fig. 9.c) is structured with two parallel switches. The output of the NAND gate will be positive pressure (1) as long as either one or both of the two switches open (input is 0).

OR, AND. By adding a successive NOT gate to NOR gate, we can get an OR gate (Fig. 9.b). Likewise, AND gate can be constructed by adding a NOT gate to NAND gate (Fig. 9.d).

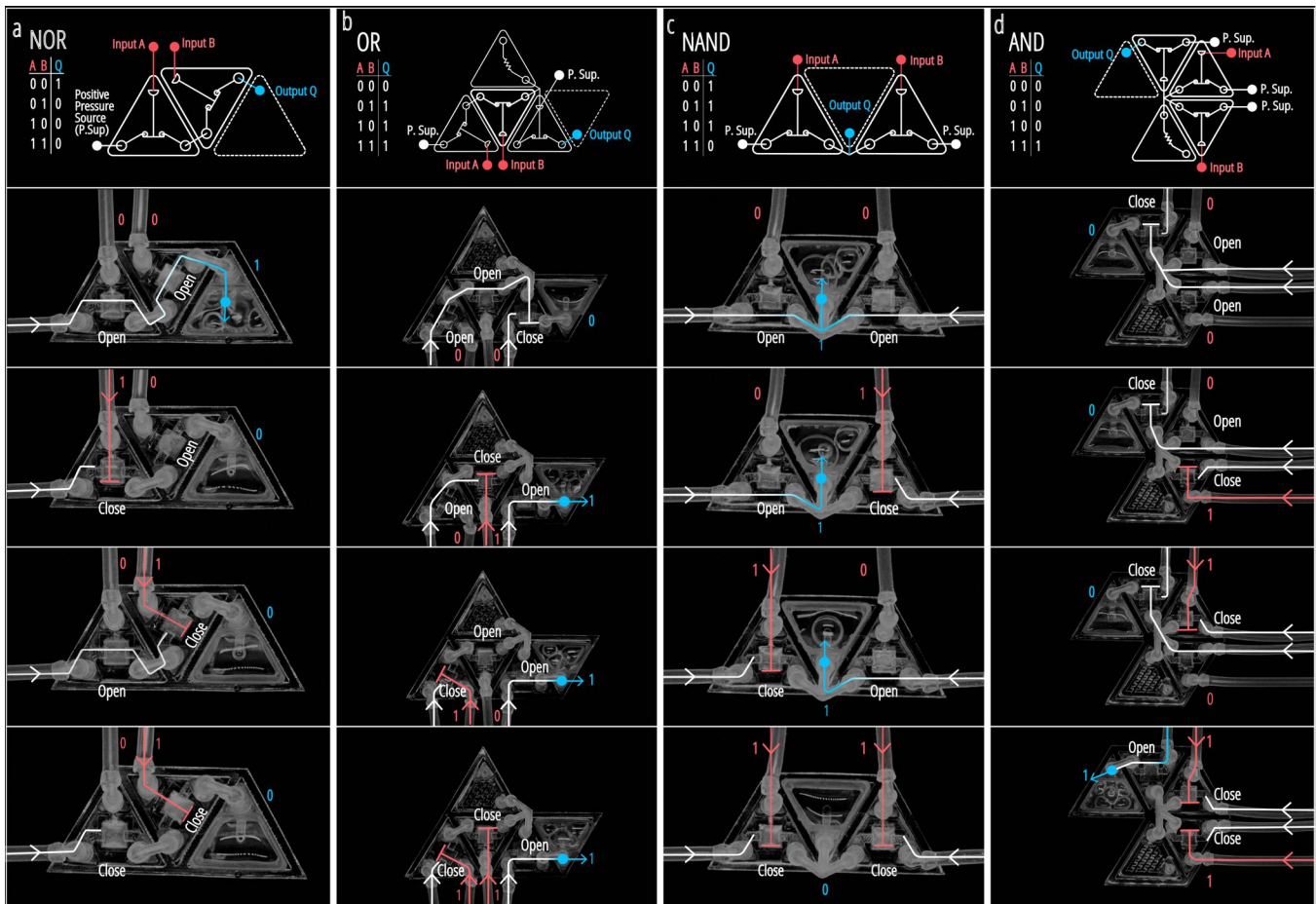


Figure 9: The output variations of the fluidic logic gates depending on their input: a) NOR, b) OR, c) NAND, d) AND. Magnets are removed to show the membrane deformation more clearly. In this case, higher control channel pressure is required to block the target channel.



Figure 10: The fluidic filter. a) Design diagram of the capacitor. b) (Left) When the capacitor is squeezed by the input, the left diode is blocked and the airflow is released from the right diode; (Right) When the capacitor is rebounded, the left side diode is fed and the right side diode is blocked.

4.3.2 *Filter*. In this subsection, we present the design of a bandpass filter (Fig. 10). This operator's output flow rate varies with the input force signal frequency. The output airflow will peak when the force is input at a specific frequency and decrease as it deviates from this peak frequency. The filter is a completely passive device, which means it will work as long as there is input airflow and won't

require a constant positive pressure air supply like in the logic gates. The core component of our filter design is a capacitor that can pump air out when deformed by external force and self-restore after the external force is removed.

With this design, the lowest frequency that can pass through the bandpass filter is determined by the volume of the capacitor,

and the upper cutoff frequency is generally proportional to the total resistance of the hardware component. The filter component in conventional fluidic computational devices is rather complex and handles a wide range of frequencies from 0.01 Hz to 100 Hz [7]. Here we came up with a much simpler yet effective design with only one capacitor, one resistor, and two diodes to tailor to human input with a relatively limited deformation level control and low frequency. Further, by tuning the capacitance of our capacitor component and the total resistance of our resistor component, we can tune the frequency range the filter can pass through. The later Performance section shares more detailed design considerations and performance characterization.

4.3.3 Timer. A timer operator is a relay with a time delay built in. After receiving a positive air pressure signal, it will pass down the signal after some time delay if the signal is still there. A timer is also a passive operator that requires no constant positive pressure air supply.

A timer consists of two resistors, one capacitor, and one switch (Fig. 11). The resistor 1 (R1) connected with input is used to reduce the flow rate. Since the capacitor works as a buffer that delays the pressure building up in the system, a thin, soft plastic airbag is chosen. The switch will only connect when the target channel reaches its bursting pressure to ensure that the output signal remains 0 until the capacitor reaches the switch's pressure

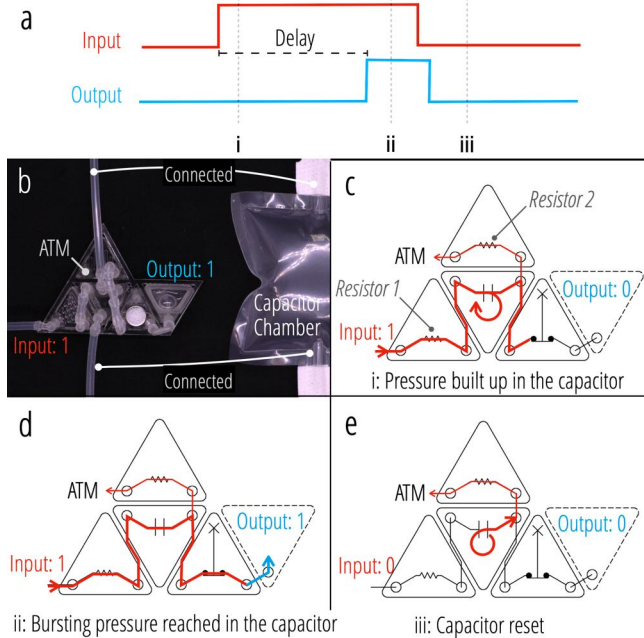


Figure 11: The fluidic timer. a) Input and output signals. b) Functional prototype. c-e) The signal changes through three phases from i (pressure built up inside the capacitor), ii (bursting pressure reached in the capacitor) to iii (capacitor reset after one triggering cycle)

capacity. A vent is included to ensure the capacitor can reset automatically after the input signal drops to 0. The resistor 2 (R2) is connected with the vent and works as a pull-up resistor.

We use two approaches to regulating the delay time. One is by changing the total resistance of R1. Increasing R1 will further decrease the flow rate, thus extending the delay time. However, a more resistive R1 also means more pressure drop. So if the output signal of the timer needs to be fed to successive circuits, raising the resistance may not be a good choice. The other approach is to increase the capacitance of the capacitor component [8], which is usually better than the first approach, except less compact. Regulating R2 can change the resetting speed of the capacitor. Lowering R2 will decrease the restoring time. However, this also means more pressure loss will occur. Though not used, the third possible approach to regulate the delay time is tuning the bursting pressure [6]. It is possible with our Kit, as the bursting pressure of the switch can be adjusted by changing the top magnet.

In short, if a positive pressure or high flow rate is required for the output, choosing a low R1 and a high R2 is recommended, in which case, the delay time can be regulated by changing the capacity. Timer designs with different design parameters are further evaluated in the later Performance section.

4.3.4 Register. The register is a storage unit that can store one bit of input force data. We can use it to record input, or maintain output when the input signal is gone. In our Kit, the register is achieved with a fluidic D-latch. The core part of a D-latch is a bistable flip-flop structure. The flip-flop has two switches that will stay in two opposite states. As shown in (Fig.12.a), when the left switch gets unblocked, air will feed to the bottom channel of the right valve and block it; vice versa, when the left switch is forced to close, the right valve will open (Fig. 12.b).

D-latch can be constructed based on the flip-flop. As shown in Fig. 13, it can receive one input data signal (D), and one input control signal (E), and can give two opposite output signals (Q and inverted Q: \bar{Q}). The input signal can only be written when the input control signal is 0. Moreover, data will be locked and stored

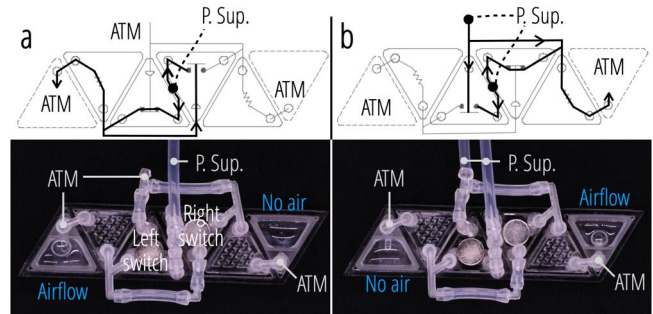


Figure 12: The core structure of a D-latch: the bistable flip-flop. a) When 0 (ATM) is given to the control channel of the left switch: left switch unblocked, right switch blocked; b) when 1 (positive pressure) is given to the control channel of the left valve: left off, right on.

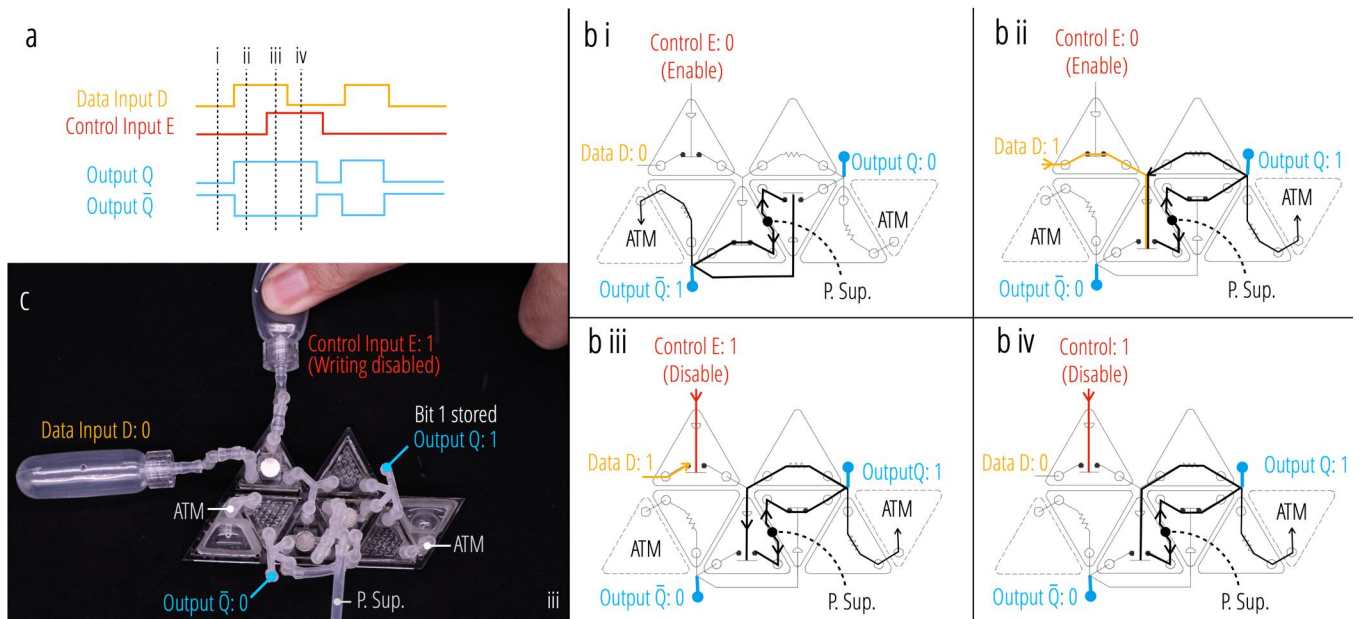


Figure 13: The fluidic D-latch. a) Output variations depending on data input and control input. b) The input data signal can only be written when the input control signal is 0(i to ii) and data will be locked and stored after the input control signal changes back to 1 (iii to iv)

after the input control signal changes to 1. The output Q is the same as the stored data, while the output \bar{Q} is opposite to the data.

D-latch is very different from the other operators because when output is not connected to a successive circuit, it needs to be sealed instead of left open to the ATM. So in Fig. 13, we seal both outputs and use the tub connected with the vents to show the status.

D-latch can receive input data either from the user-manipulated airbag or preceding operators. When an airbag is connected, the airbag will not reverse properly if the input control signal disables data writing because there is no other port to let the airbag suck air in. In this case, the airbag must have another one-way inlet to restore air. In Fig. 13, we drill a hole that will be blocked when it gets pressed by a finger to achieve the same function as a one-way inlet.

4.3.5 Edge detector. The edge detector operator can monitor the input signal and generate a short air pulse at the output when a rising or/and falling air pressure occurs at the input.

In Fig. 14, we demonstrate a rising edge detector. It is constructed by adding switches and resistors to a NOR gate. And one additional magnet is placed on the bottom right switch to lower the pressure threshold of blocking its target channel. Fig. 14.d explains that states of the operator at different phases i-iv: i) The default state when both input and output are 0. ii) when the input signal changes from 0 to 1, the left NOR gate switch will open instantly, which induces a 1 (a quick positive pulse) at the output. iii) After a very short while, the right NOR gate switch gets blocked due to the air pressure building up in its control channel, which turns the output from 1 back to 0. iv) When the input signal changes from 1 back to 0, the left NOR gate switch will be blocked instantly, thus keeping the NOR gate output 0.

For applications requiring an extended pulse duration at the output when a signal is detected at the input, we can replace the resistor $R1$ (shown in Fig. 14.d i) with a capacitor. The alternative design with an additional capacitor is shown in Fig. 15. Besides, by adding an inverter to the input port, we can get a falling edge detector.

4.3.6 (De)multiplexer. The demultiplexer is 1-to- 2^N , which means the single input source signal can be steered to any of the 2^N outputs by applying N input controls. In Fig. 16, we demonstrate a 1-to-4 fluidic demultiplexer with one source signal, two input controls, and four outputs. It consists of ten switches, two resistors for venting, two rubber air blowers to perform control inputs, and four tubs to visualize the outputs (Fig. 16.a). Each input control is split into two, with one of them inverted by the NOT gate. Therefore, though there are only two input controls, we can get four combinations of inputs. The working details of the demultiplexer are illustrated with Fig. 16.a and b.

The demultiplexer can be used to connect a single source to multiple destinations. We can leverage demultiplexers to give users 2^N different outputs by receiving only N control inputs. The demultiplexer can also be used to build complex circuits, e.g. we can set the source signal port to receive the user's input, steer the user's input to each outputs by changing the control signal periodically, and store the outputs by connecting each outputs to a register. Then we can build a fluid computation system that records the user's inputs, and the record can be displayed by connecting to output airbags.

When operating reversely, the demultiplexer can become a multiplexer, which can select and route any of the several source signals to a single output. A multiplexer shares a similar mechanism with the demultiplexer.

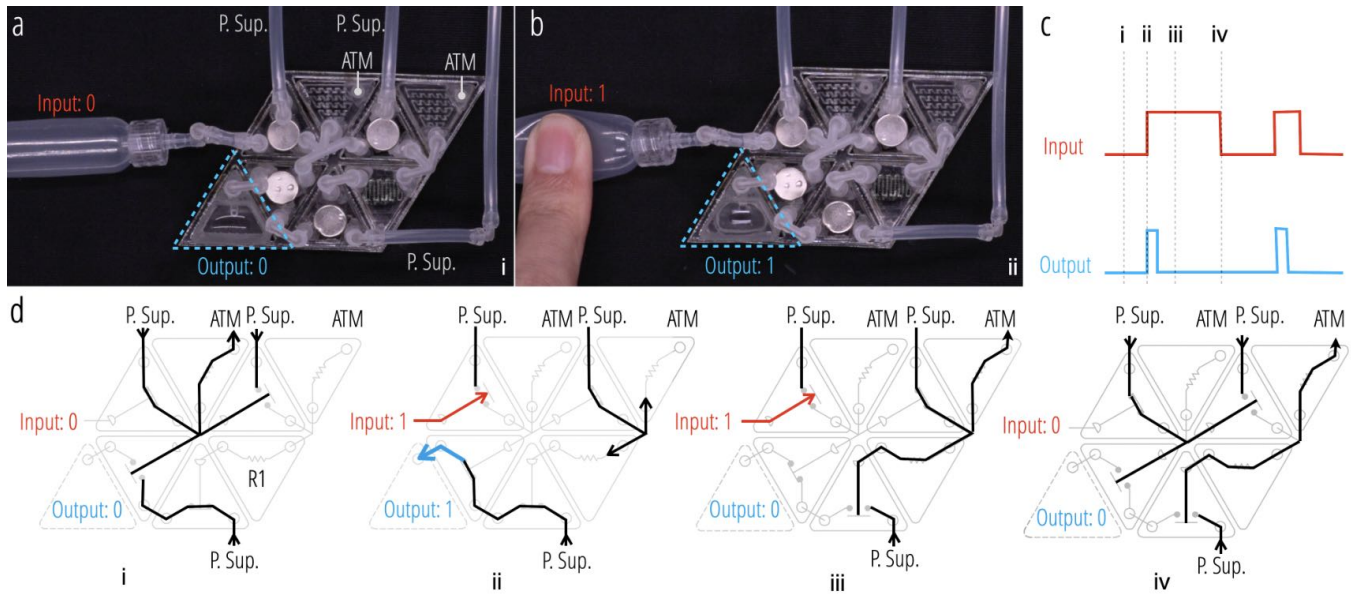


Figure 14: A fluidic rising edge detector that generates a short air pulse when a rising input pressure is detected. a) No output when there is no input signal. b) The output turns to 1 (with positive air pressure) briefly when a rising edge signal is detected at the input. c) Output variations depending on input changes. d) Sequential operation of the edge detector. The signals and corresponding valve states are listed for each stage from i to iv corresponding to (c).

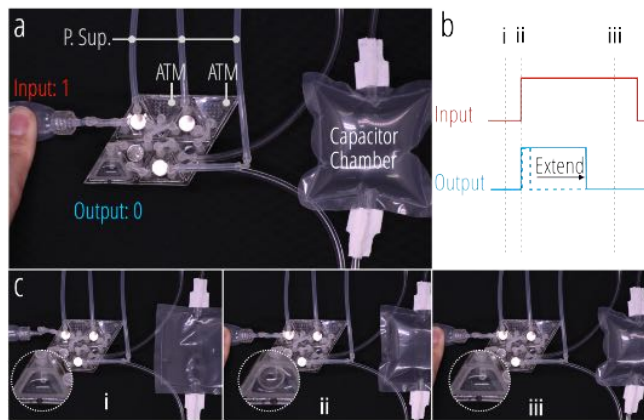


Figure 15: An edge detector with an extended duration of pulse at the output. a) Edge detector with an additional capacitor replacing the original resistor R1. b) Output variations depending on input. c) Sequential operation of the edge detector with a capacitor. The signals and corresponding valve states are listed for each stage (i to iii)

The (De)multiplexer is also considered a passive operator. It does not require the P. Sup. to be functional. As shown in the aforementioned complex circuit example, the source single does not necessarily need to be connected to a positive pressure air source.

4.4 Input/Output devices

4.4.1 Designing the input devices. The basic principle for designing an input device is that it should be able to convert the force changes of interest to air pressure changes. Typically, airbags are good candidates. Based on this principle, we proposed the following guideline if airbags are used as the input devices:

- The form factor should match the context and user’s action, e.g., cylinder airbags are suitable for squeezing; small flat airbags are easily activated by pressing with the finger, and large flat airbags are best utilized by pressing with the whole hand.
- The airbag should have only one port connected to the input port of the computation circuit; it should not have another port connected to the atmosphere.
- If utilizing flat airbags, for example heat-sealed plastic bags, an appropriate amount of air must first be injected into the airbag before it is connected to the circuit. If using 3D airbags that can restore automatically after the forced deflation (e.g., hollow silicon airbags), then the pre-air-injection is not necessary.
- In some cases, the capacitor will act as both the input device and computational components (e.g., in the filter). The capacitor has its own design standard, as described earlier.

4.4.2 Designing the output (devices). The output air flow of the circuit can be converted to many output modalities, for example:

- Shape and texture change. Technically, most inflatable shape-changing output devices designed by prior work can be directly connected and controlled by our fluidic computation circuit, providing rich shape-changing feedback for various

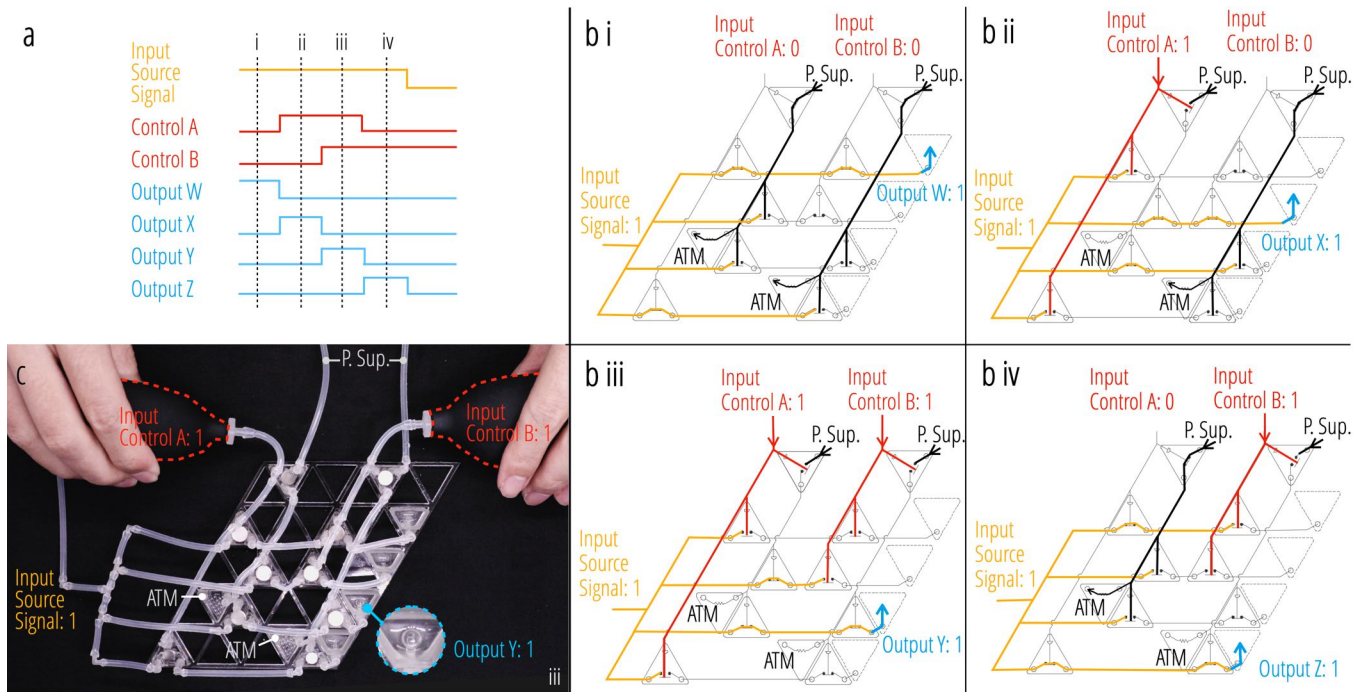


Figure 16: The fluidic demultiplexer design and working mechanism. a) Output (W to Z) variations depending on two controls (A and B). b) The demultiplexer’s I/O signals and corresponding switch states are listed for each stage (i to iv). c) When both input control signals are 1, output Y gets selected.

scenarios. It is worth mentioning that the fluidic computation circuit can only operate at 1 or 0, so it can not provide negative pressure to actively deflate these shape-changing airbags. Therefore, the shape-changing airbag must have a vent. The vent can be connected to a resistor to regulate the venting rate to ensure the airbag can be fully inflated when the output signal is 1.

- Haptic. Aside from pneumatic shape and texture changes that can be used to provide haptic feedback, airflow can also directly induce haptic experiences. We can easily tune the haptic feedback strength by adjusting the flow rate with the resistor, adjusting the haptic feedback area by changing the shape of the air outlet, or creating morse code style haptic feedback with 1 and 0 output signals.
- Sound. The airflow can generate sound, e.g. by blowing a wind chime or blowing up an airbag.
- Scent. The airflow can carry the scent. e.g., Essential oils can be dripped onto the capacitor and travel with the airflow to deliver scent when circuit output is 1.

5 EXAMPLE CIRCUIT AND APPLICATION

Sophisticated interaction systems can be built with our Kit. This section showcases four example fluidic circuits integrated with various input and output devices for different application scenarios. Among them, two passive systems do not require an air compressor as a positive air pressure supply, thus completely electronic and air-tank free.

5.1 Force Encrypted Passive Latch

We designed a force-frequency encrypted “safer lock” that takes force frequency as the input, uses a customized filter to compute and actuates a bendable airbag as the output. The latch can only be opened when the capacitor is pressed at a programmed frequency. This latch can be used in, for example, a medicine drawer that can prevent kids from opening it accidentally.

A rubber air blower is modified to work as the deformable chamber of the capacitor components and the door handle. Only one diode is used because the air blower has a built-in check valve structure. The peak frequency of the filter is tuned to around 1 Hz with the resistor. The bendable airbag has a vent hole reserved. As illustrated in Fig. 17, the airbag will only reach maximum bending when the door handle is squeezed at a frequency near 1 Hz.

5.2 Self-contained Passive Wake-Up Alarm

We designed a self-contained wake-up alarm powered by force applied by the user (Fig. 18). It takes force duration as the input, uses a customized timer to compute, and outputs haptic and scent feedback to users.

When the user takes a nap, a fresh breeze will wake the user with a gentle touch and delightful scent at a 5 minutes mark.

An inflated pillow works as the input device. Its port is connected to a customized timer operator’s input port. The capacitor and resistors are tuned to make the delay last around 5 minutes. A small amount of essential oils is injected into the hexagon airbag. Finally, a small adaptor is connected to the output outlet to turn

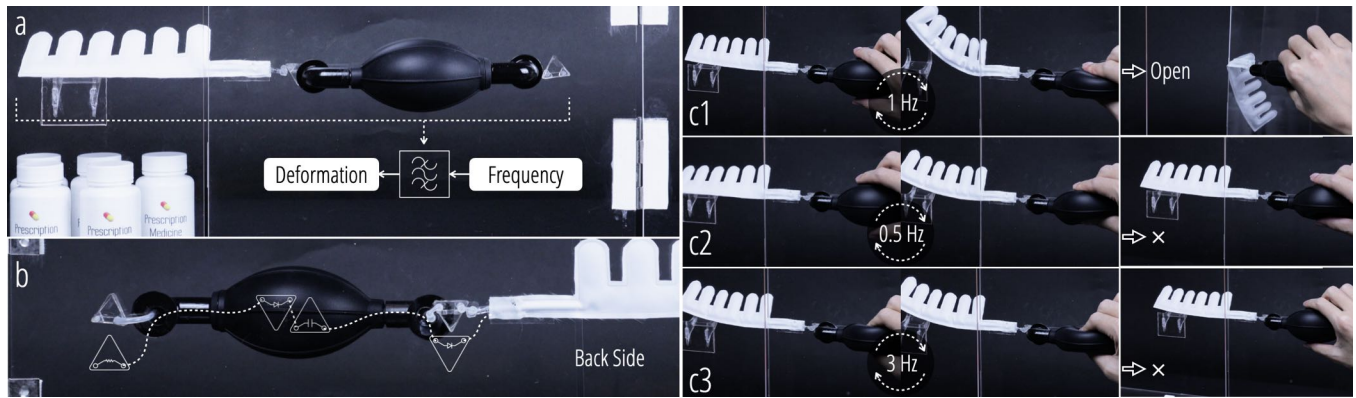


Figure 17: A force encrypted passive latch. a) The overview. b) The computational circuit. c) The user input signals and corresponding balloon states are listed for each round.

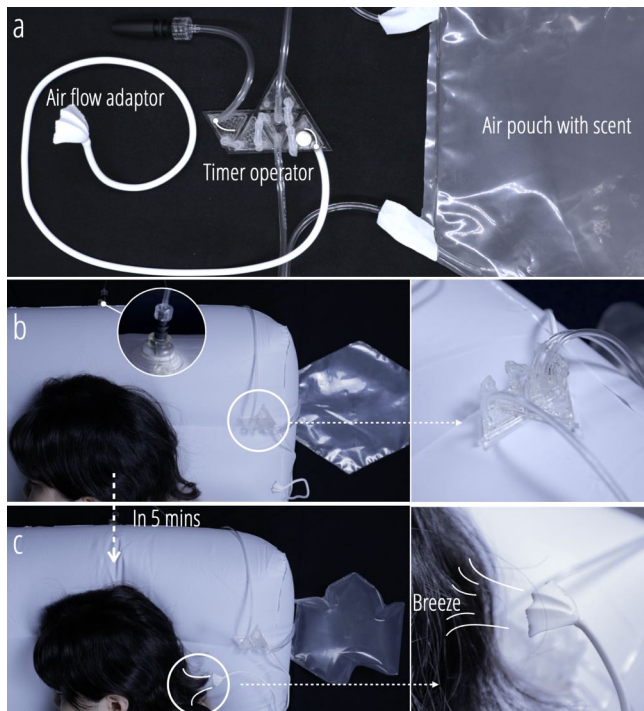


Figure 18: A self-contained passive alarm with a pillow as an input device. a) The overview. b) The alarm’s input computation module is composed by the Kit. c) The alarm’s output performance from the computation module.

the cylindrical airflow from the circuit output into a flat, gentle air stream.

5.3 Posture Detection and Correction Chair

By simply mounting a fluidic computation system to a chair, we enhance the chair by adding the ability to monitor sitting positions and alert the user when a poor posture is detected.

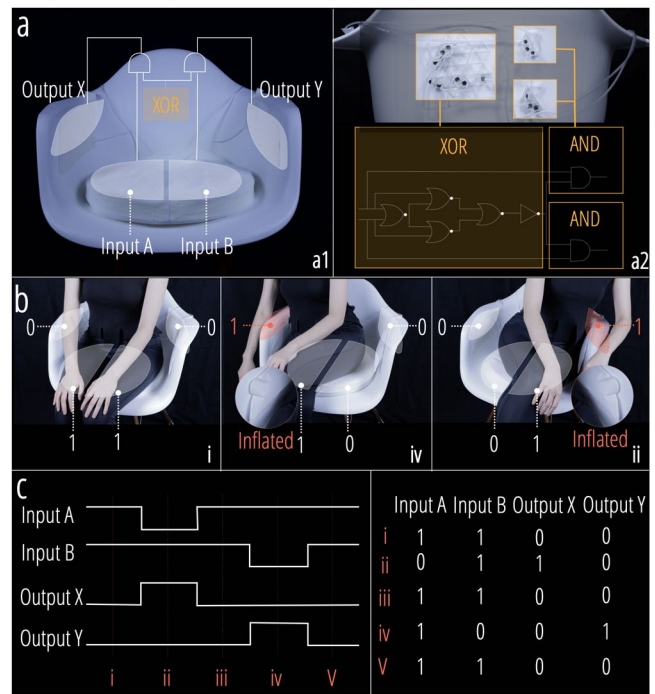


Figure 19: The posture detection and correction chair. a) The logical diagram and the computational module mounted at the back of the chair. b) The user input signals and corresponding chair states are listed for each stage (i to iii) c) Output variations depending on user input.

As illustrated in Fig. 19.a1, the chair has two airbags embedded in the cushion to detect force distribution, a fluidic computation module adhered to the back, and two airbags mounted to each side of the chair to provide output feedback.

The computation module is constructed with one XOR gate and two AND gates (Fig. 19.a2). XOR consists of four NOR gates, and will output 1 when two inputs differ. So when the user is leaning to

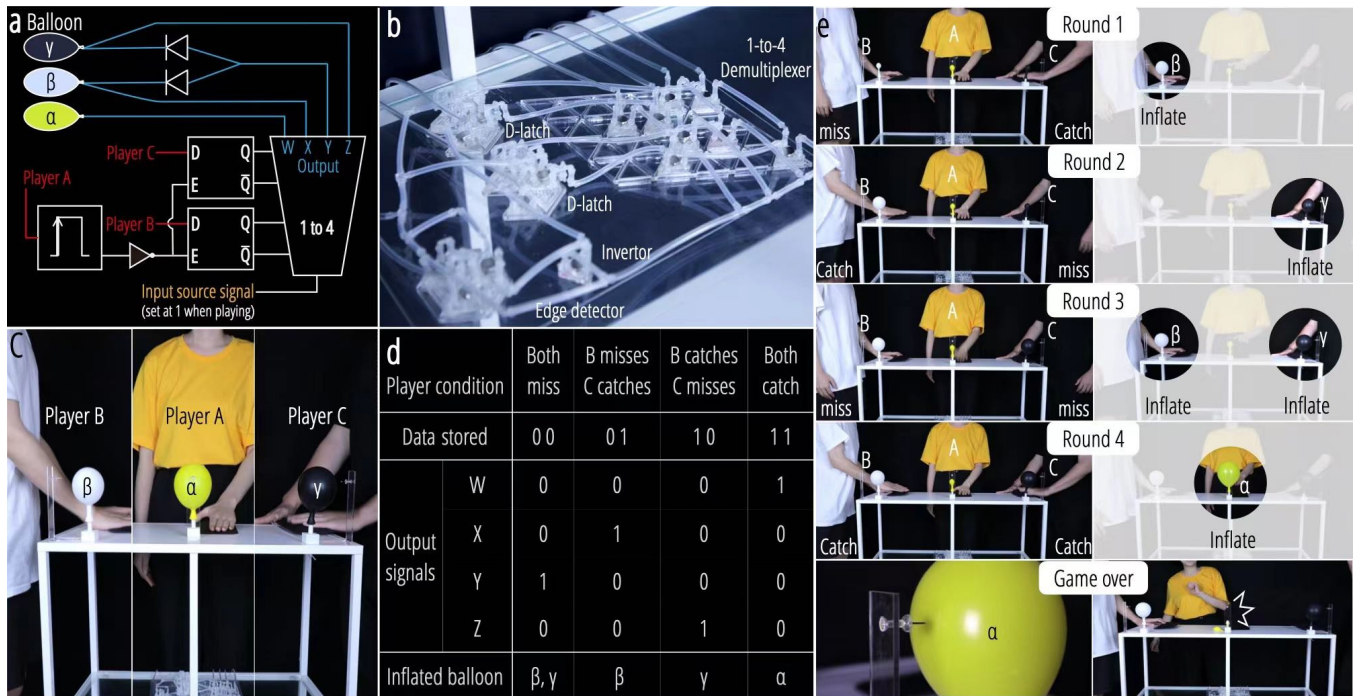


Figure 20: a) Circuit diagram and I/O of the multi-user rhythm game with the Kit. b) Computation module composed by the Kit, diodes are placed in the balloon bases separately c) Game setup with three players, three air bladders on the table as the inputs, and three inflatable balloons as the outputs. d) Output variations depending on the input from the players. e) The user inputs and the corresponding balloon states are listed for each round.

the right or left side, the two input signals will differ and XOR will output 1. Then the two ascended AND gates will process the signals from XOR and two inputs, deciding which output airbag should be inflated to remind the user to maintain a good sitting posture. When the user is not sitting on the chair (both input signals are 0) or sitting upright (both input signals are 1), the output airbags will remain un-inflated.

Moreover, if designed with proper size and stronger output airbags, we think such a smart chair can also provide leaning protection for children, elderly, or paraplegics.

5.4 Multi-user Rhythm Game

We deployed a multi-user rhythm game with the Kit. The system can take and store inputs from three users, execute parallel computation, and give different outputs accordingly.

As illustrated in Fig. 20, the game system has three input airbags, a fluidic parallel processor module, and four outputs visualized with three balloons. The computation module is constructed with one edge detector, one NOT gate, two d-latches, one 1-4 multiplexer, and two diodes.

Whenever player A suddenly hits airbag A, the edge-detector will generate a short signal 1 that lasts for 500ms. This short signal 1 is then inverted by the NOT gates to a short signal 0. And this short signal 0 is fed to the control input of the successive two d-latches, enabling the d-latches to receive data while this short signal 0 lasts.

If players B and C hit their airbag within this short time window and hold until the short signal 0 is gone, then bit 1 will be written and stored at d-latches. Otherwise, bit 0 will be written and stored. A successive demultiplexer has its input controls connected to the two d-latches outputs, and it will decide which one of its four output signals will be 1 based on the stored data by the d-latches. Fig. 20.e shows different combinations of the player's inputs and the corresponding balloon states as the outputs. The one whose balloon explodes first will lose the game.

6 FABRICATION

In this section, we explain the details of the design and manufacturing process.

Design and Modeling. The components, especially the switch valve, are carefully designed. The form factor and the function of the magnets have already been explained. For the top and bottom layers, we chose acrylic that can be easily laser machined. In the middle, we embed a composite membrane module made of a strong double-sided tape (3M 4905) and two 0.1mm thick TPU squares. When the air pressure change induces the tape to deform, TPU squares can prevent the tape from irreversible plastic deformation or adhering to the wall of the functional channels on the acrylic layer. TPU squares come in different sizes because slightly enlarging the lower TPU squares can ensure air-tightness when the target channel gets blocked. Components and accessories are modeled

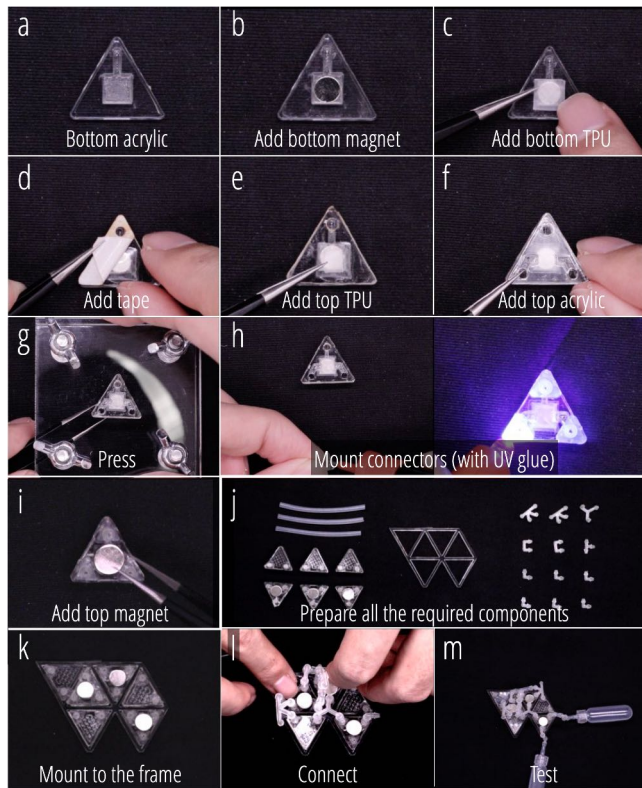


Figure 21: Components assembly and wiring process. (a-i) Assembling a switch. (j-m) Assembling an operator through wiring components.

with 2D or 3D modeling software like AutoCAD and PTC Creo. All model files can be found in the supplementary material.

Raw Material Processing. The Acrylic, TPU, and tape are machined with Universal Laser Systems’ Ultra X6000. The connectors are printed with a Formlab SLA printer. The detailed settings are available in the supplementary material.

Components Assembly. As demonstrated in Fig. 21.a-i, the switch can be assembled layer by layer. Other components follow the same procedure but with fewer layers. To maximize the bonding strength of the tape, we designed a press tool to clamp the components at step Fig. 21.g. The success rate of manually assembling the switch was 80%, then raised to above 90% after introducing a 6mm thick triangle laser-machined mold to help align the layers and act as the height limit block to precisely control how much the press tool will press. The model file of the mold is provided in the supplementary material.

Circuit Wiring. The components can be wired to get complex circuits (Fig. 21.j-m). To facilitate the wiring process, we designed some frames and connectors. The frame can help to fix the computational components, and various connectors are used primarily to split the path of the air and secondarily to create efficient routes.

Number	1	2	3	4	5	6	7	8	9	10	Avg.
Pressure Drop (kPa)	0.45	0.23	0.39	0.28	0.21	0.30	0.51	0.49	0.33	0.27	0.32

Table 2: Pressure drop test results of ten switches. Tested switches have a D 8mm × H 2mm circle magnets on the top. Target channel inlet pressure is 15 kPa.

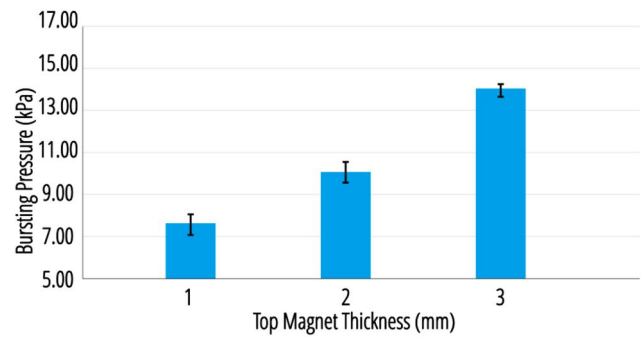


Figure 22: Bursting pressure test results of the same ten switches of table 2.

7 PERFORMANCE

The performance test results of our Kit are discussed below. In this section, we present the detailed results of the performance tests for selected components and operators during the design process.

7.1 Components Evaluation

The switch, resistor, and diode are evaluated. The performance of the capacitor is included in the filter and timer evaluation in the next sub-section.

7.1.1 Switch Evaluation. As mentioned, the switch valve has a pair of magnets, giving it a static gain property. The target channel will remain blocked before the air pressure applied to it increases beyond the threshold (bursting pressure). In addition, we mentioned that a very low resistance design is critical in designing cascading switches. Therefore, we carried out experiments to evaluate our design’s resistance and bursting pressure. Table 2 shows the pressure drop between the target channel inlet and outlet of ten of all the qualified switches.

One reason the resistance ends up being extremely low is that once the switch is burst to open, the magnetic force will dramatically decrease as the force is inversely proportional to the distance squared. Fig. 22 shows the bursting pressure test result of the ten switches mentioned above. The bursting pressure can be easily tuned by changing the magnets. Unless otherwise stated, all operators and advanced circuits in our paper are constructed with switches that have an 8 mm × 2 mm (diameter multiply height) top magnet and a 5 mm × 1 mm bottom magnet. Again, that is why in our system, the signal is usually considered as 1 when it is above 10 kPa. Fig. 23 demonstrates the test result of the blocking pressure of the switches, as mentioned earlier, under various conditions. It

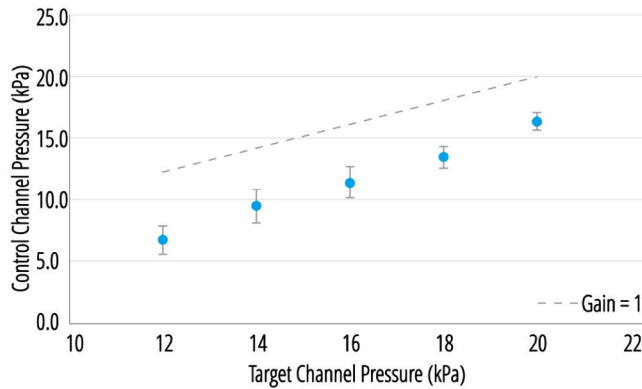


Figure 23: Blocking pressure test results of the same ten switches of table 2.

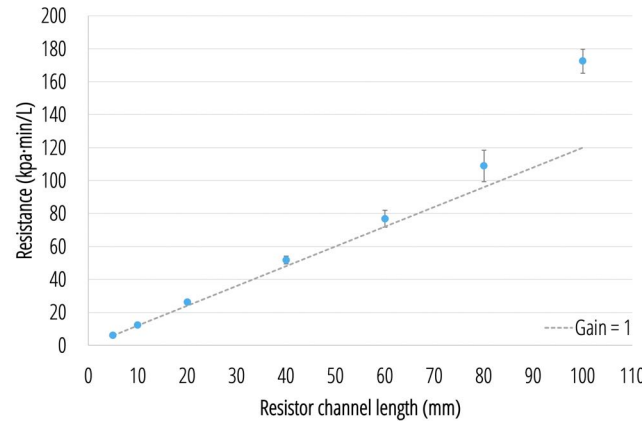


Figure 24: The resistance measure results of our resistor collection. Each resistor was tested under flow rates of 0.5, 0.75, and 1L/min. The inlet and outlet air pressures are measured to get the air pressure drops value for calculating the resistance. The dotted line is measured and plotted with resistors that have straight, unfolded channels.

is evident that, with the help of magnetic force, the control channel can block the target channel easier.

7.1.2 Resistor Evaluation. Since the resistor components are very compact, we have to fold the narrow channel up to 100mm in length to fit. To measure the resistance and verify if it still changes linearly to the length, we carried out the following experiments.

We tested the resistors with (equivalent) channel lengths of 5, 10, 20, 40, 60, 80, and 100 mm. Since the minimum distance between inlet and outlet is already greater than 5mm, the equivalent 5mm resistor is enabled by having two 10mm channels in parallel.

The results show that overall the resistance is proportional to the length (Fig. 24). The gain^{1, 2} of the length variation (5mm - 80mm) on the resistance variation is approximately 1. This stable

¹The Gain block multiplies the input by a constant value (gain)

²<https://www.mathworks.com/help/simulink/sref/gain.html>

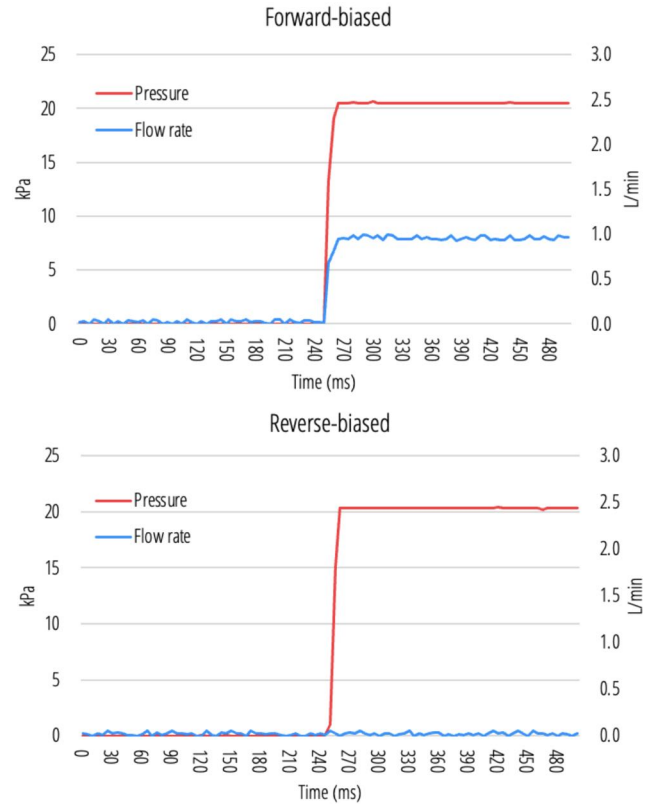


Figure 25: The diode's flow rate - pressure curves under 20 kPa.

gain appears until the length becomes 100mm. We assume that the dramatically increased internal inflection of the 100mm resistor caused by the folded narrow channel is responsible for the gain fluctuation. Also, this fluctuation might be one of the main reasons why our experimental results are not perfectly linear. Nevertheless, we still believe that by changing the narrow channel length, we can tune the flow resistance in a very controllable way. That is, when designers use the Kit, they can choose the right resistor or combine different resistors based on their needs.

It is worth noting that the resistor in our fluidic computational system can only be analog to the electrical resistor when the flow through it is in its laminar regime [38]. When the flow becomes turbulent, the resistance variation will no longer be linear thus making it difficult to predict.

We can also calculate the flow state through the resistor in our Kit. Reynolds number is the main indicator used to distinguish turbulence and laminar flow. Normally, laminar flow occurs when $Re < 2300$ and turbulent flow occurs when $Re > 2900$ ³. We calculate the Re with Equation 1, where ρ is the density of the fluid (kg/m³), u is the flow speed (m/s), d is the channel diameter, and μ is the viscosity coefficient of the fluid (Pa·s). In addition, since in our Kit the channel is not cylindrical, it is necessary to calculate the

³https://en.wikipedia.org/wiki/Reynolds_number

equivalent diameter(de) with the Equation 2. Here, A is the cross-sectional area and L is the perimeter. For our resistor, A is $0.5m^2$, and L is 2.24 mm, hence the de is 0.89 mm

$$Re = \frac{\rho u d}{\mu} \quad (1)$$

$$de = \frac{4A}{L} \quad (2)$$

In our system, the Reynolds number is only affected by the flow rate variation, so the designer can check the flow via different flow rate parameters as needed. For example, at a flow rate of 1 L/min, the Reynolds number is calculated as 712, which is much less than 2300. That is, the flow in the resistor is in the laminar regime.

In this paper, all the circuits operate between 10 kPa and 30 kPa with the flow rate below 1.5L/min, which means no turbulent flow appeared in our circuit.

7.1.3 Diode Evaluation. The diode's flow rate - pressure curves are measured under 20 kPa. As shown in Fig. 25, it allows air to flow easily in one direction but severely restricts air from flowing in the opposite direction.

7.2 Operator Design Consideration and Evaluation

7.2.1 The filter. Filter component has been previously deployed in microfluidic chips, yet with a quite complicated structure [29]. In addition, microfluidic filters are verified by using a motor or a pump to generate a constant force/pressure signal that is applied periodically in a wide range of frequencies (from 0.01Hz to as high as 100Hz) [7]. With these well-controlled signals, the degrees of deformation of the capacitor is different under different frequencies. However, when it comes to human operations, we hypothesized that 1) It is very hard for people to perform constant force/pressure, and instead, people tend to press the capacitor to its maximum deformation; 2) It is also difficult for people to operate at higher

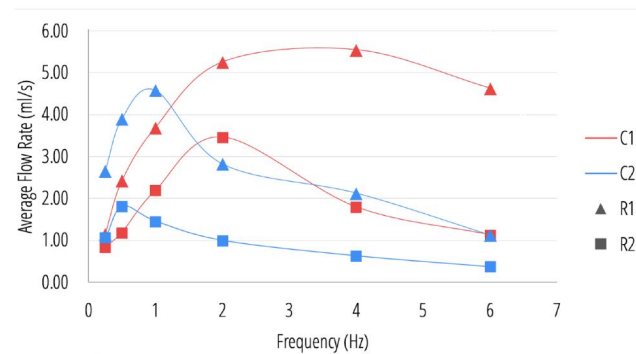


Figure 26: The average flow rate under different actuation frequencies measures results of four filters (C1:80% rebound in 0.25s , C2: 80% rebound in 1 s, both have a hollow cylinder chamber that diameter is 3 cm and height is 1.5 cm. R1: 5 mm and R2: 20 mm) at different frequencies. The top layer of the filter is pushed against the bottom every time.

than 10 Hz due to physiological limitations. This may pose unique criteria for our filter design.

To preliminary verify our hypothesis, we did a pilot user test with the capacitor shown in (Fig. 10), which is made of silicone and has a hollow cylinder structure and elastic top. Four people are asked to press the capacitor with their fingers under 0.25 Hz, 0.5 Hz, 1 Hz, 2 Hz, 4 Hz, and the maximum frequency they can reach. They all pressed the capacitors down to the bottom without many degrees of deformation control, especially under high frequency. Moreover, the maximum frequency they can achieve is approximately 6 Hz.

Based on these features of human operations (limited deformation control at relatively low frequencies), we design a simple yet practical bandpass filter that only requires one capacitor, one resistor, and two diodes. As shown in (Fig. 10), we consider the force applied to the capacitor as input and the airflow from the diode as output. The input frequency will affect the deformation of the elastic top of the capacitor, thus changing the air supply to the diode. Therefore, by observing the airflow from the output diode, we can determine the filter's response to the frequency.

Theoretically, for filtering at different input frequencies, the elastic top's deformation capacity and the capacitor's volume are generally proportional to the magnitude of the lower cutoff frequencies in the bandpass filter. This is because these two factors' magnitude may affect the air supply's continuity to the diode in low-frequency states. However, on the other hand, the resistance is generally proportional to the magnitude of the upper cutoff frequencies. This is because the resistance may affect the ability of the capacitor to pump air at high frequencies, which may cause the elastic top to fail to deform or rebound in time.

We conducted a quantitative experiment to measure the effect of different capacitance-resistance filters on the airflow from the diode at different frequencies (Fig. 26). The results show that the peak frequency of the bandpass filter is correlated to the resistance and the deformation capacity of the capacitor, as we expected. Therefore, we believe that by changing the capacitor in deformation capacity or the value of resistance, we can tune the bandpass filter in a

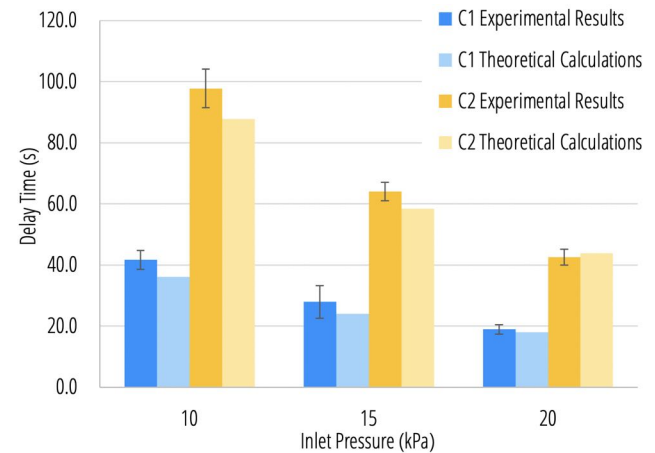


Figure 27: The delay time measure results of four kinds of timer at different inlet pressure

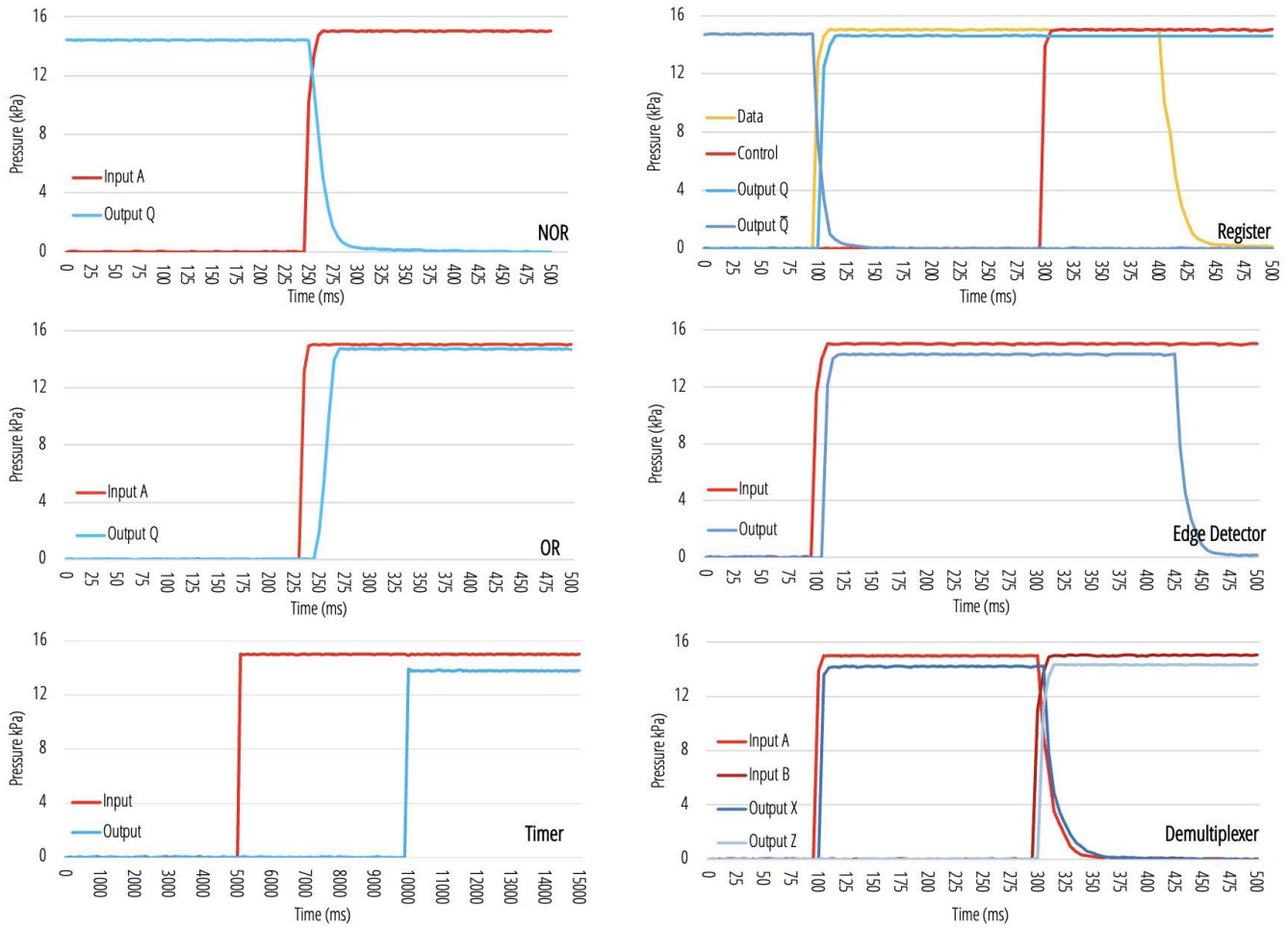


Figure 28: The representative pressure traces of operators, among which the timer counts 5s, the edge detector outputs a 300ms signal when a rising edge is detected.

controllable way. That is, when designers use the Kit, they can filter the user input on their needs.

We tested four filters composed of two capacitors (cylinder hollow structure with 3mm diameter base) with different deformation capabilities. The results show that overall the peak frequency of the bandpass filter is correlated to the resistance and the deformation capacity of the capacitor. Specifically, the results of comparing filters C1R1 and C2R1 verify our previous theory of the lower cutoff frequencies well. With almost no additional resistance in the filter channel, we can increase the peak frequency of the output airflow from 1hz to 4hz by adjusting the capacitor deformation and rebound capability. Also, by comparing the effects of different resistances (C1R1 & C1R2, C2R1 & C2R2), we find that a large resistance reduces the rebound speed of the elastic top, thus lowering the peak frequency of the output airflow. This also supports our previous theory on the upper cutoff frequencies.

Therefore, we believe that by changing the capacitor in deformation capacity or the value of resistance, we can tune the bandpass

filter in a controllable way. That is, when designers use the Kit, they can filter the user input on their needs.

7.2.2 Timer. To validate our design that regulates the delay time by changing the capacitor only, we carry out the following experiment. Two timers based on capacitors of different volumes (volume at breakthrough pressure: C1 = 35ml, C2 = 85ml) were selected and tested under three experimental conditions of inlet pressure. And the theoretical delay times are calculated with Equation 3. Here v is the volume of the capacitor when it reaches breakthrough air pressure, p is the inlet air pressure, and r is the resistance.

$$t = \frac{vr}{p} \quad (3)$$

The comparison of experimental and theoretical results is shown in Fig. 27. The capacitor's volume is proportional to the delay time, which is basically in accordance with our design, but can be a little higher due to the capacitor is connected to a venting resistor.

7.3 Cascadability Evaluation

In Fig. 3 c, We preliminarily demonstrate the cascadability of the system with two switches. We carry out more experiments to evaluate the cascadability quantitatively. The input and output air pressure traces of operators are measured under the condition that the positive air pressure supply and input air pressure are set at 15 kPa.

The representative results are plotted as shown in Fig. 28. Some similar results are omitted; for example, the output air pressure of the NOR gate behaves almost identically when either of the two inputs' air pressure changes. For all the tested operators except the timer, the pressure drops of the output vary from 0.26 kPa to 0.79 kPa. The dropping value is related to the property of the switches (Table 2). Such pressure drops will not accumulate if the successive operator is not passive. Moreover, based on the results of Fig 22, it is evident that the output pressure is high enough for the successive operator.

The timer is slightly different from the others. We test a 5s timer that has a small resistor and the pressure drop is 1 kPa. Though the output pressure is still enough to activate the successive operator, when one wants to cascade timer with other operators, it is better to use the capacitor only to regulate the delay time.

Apart from the timer, the output latency is generally between 10 ms to 30 ms. Such latency can accumulate as operators are chained. However, since it is very small, it generally will not interfere with the normal operation of the system.

8 DISCUSSION, LIMITATION & FUTURE WORK

8.1 Availability and Applicability

Availability: The Kit can be fabricated with common tools and materials that researchers, designers, and makers focusing on related fabrication areas would usually have access to. The fabrication process can be potentially simplified (e.g., using a 3D printer to print the structure of connectors and the top acrylic layer as a whole, or using a multi-material 3D printer to print the whole components once for all). However, we also find it difficult to make such research effort more accessible, as the majority of people, or even many researchers and designers, do not have experience with nor access to "common" fabrication tools.

In this paper, we take the first step to make fluidic computation accessible by introducing the Fluidic Computation Kit. To push it further, we contacted factories and evaluated the feasibility of large-scale production. The engineers provided some solutions (e.g., molding and casting) that can reduce the number of parts, simplify the assembly process, and make the Kit more affordable. We picture that in the near future, people will be able to buy the fluidic computation components just like how they purchase electronic components or LEGO pieces, to learn, build, and play with fluidic computation interfaces.

Applicability: Our Kit enables designing interfaces with more complex integrated fluidic computation compared to prior works in the HCI field [10, 34, 47]. However, mechanical computation inherently has a lower computation power ceiling than electronic computation. Fluidic computation is not supposed to be a successor to electronic computation, but it can supplement or augment the

electronics in some scenarios. We have conducted pilot interviews and brainstorms with experts have various backgrounds, and here are some initial findings:

- (1) when there is no power supply or one does not want to use electricity (e.g., because of sustainability concerns);
- (2) when electronics would be unreliable, e.g., high humidity level or wet environment, strong electromagnetic interference environment;
- (3) when trying to improve the design of an existing electronic-free "smart structure", e.g., using the filter to enhance the bottle safer lock;
- (4) leveraging the transparency and visible nature to promote the trust-building of the ubiquitous electronics nowadays and better protect privacy, e.g., when one steps on the tiles in the monitored area, he/she can see the dyed air is pressurized to and travel in a fluidic computation unit, trigger the unit to open the shape-changing cover that blocks the camera;
- (5) leveraging the physical nature to enhance the data security, e.g., building physical encryption or storage device that can not be hacked and copied via the internet;
- (6) Lastly, designing education resources to help people learn, understand and use fluidic computation, as the Kit provides a rich set of library and a clear analogy to electrical circuits.

8.2 Simulation and Design Tool

Modeling and simulation is a common approach in microfluidic chip design. The ability to provide users with simulated previews will definitely ease the prototype iterations. However, compared to the usually very well-defined structure and boundary conditions in microfluidic chips, we face a much more complex technical challenge regarding computational simulation and design. Recently, the Soft Compiler [26] demonstrated a web-based tool to help design soft circuits built with basic logic gates. The Fluidic Computation Kit enables more types of operators, but The Soft Compiler presents a promising solution that we may potentially build on. Attempting to develop simulation and design tools in the future will make the Kit more accessible and usable by many.

8.3 Beyond Force, beyond Air

Expanding the input modalities. This paper mainly focuses on human-centered fluidic computation design and deconstructing human-induced force changes as input. However, in the field of microfluidic, many other types of control methods that can induce fluidic pressure changes have been proposed, including temperature [56], light/radiation [53], chemical [16], resonance [39], or even biological organic [21]. Enabling our fluidic computation Kit to respond to more stimulus types could expand its computational ability and interaction modalities even further.

Exploring other actuation methods. Theoretically, our computational Kit can operate with water or be used underwater, achieving computational devices that are not afraid of getting wet. Besides, though we demonstrated some passive operators and application examples that do not require any external air source, the rest still require a positive pressure air source to function. It can be electronic-free if we integrate a compressed gas tank or chemicals for gas-generating reaction in our Kit. However, both of the proposed approaches can only last for a while, and the tank will make the system bulky. In the future, we will keep seeking more actuation mechanisms to push fluidic computation from electronic-free

to electricity-free. For example, leveraging context-specific fluidic sources (e.g., using air generated from stepping on an inflatable sole [36, 49] or flowing water from running creeks) might be elegant solutions for on-site interactive devices.

9 REFLECTION AND CONCLUSION

This work encourages HCI researchers to explore and embrace the unique contribution of unconventional forms of mechanical computation in HCI. While semiconductor-based electronics are powerful, we set out to explore how fluidic computation can **supplement or augment** electronics when it comes to designing physical and material-based interfaces. Looking forward, **electronic-free and/or electricity-free interfaces** based on mechanical computers could help us build sustainable and lower-powered (or powerless and self-powered) devices. Mechanical computers could also help combine input, output, and computation seamlessly in shape-changing interfaces. Using a common pipeline to design shape-changing interfaces with electronics, we often decouple sensors, computing units, and actuators (e.g., a light sensor plugged into an Arduino board that computes and controls an electromagnetic motor). In contrast, fluidic computation may provide an integrated design paradigm that allows designers to think about the design of sensing, computation, and actuation with the same structural component (e.g., pushing an air pouch to trigger a fluidic computation that outputs a shape change driven by air). Lastly, we believe the transparent computing provides more opportunities for tinkering and learning. We hypothesize that when all the computation is performed in a physical and visible form, opportunities to design playful and tangible interfaces, which help learners to grasp the concept of computation, may arrive.

ACKNOWLEDGMENTS

We want to thank Tianyu Yu for helping conduct the literate review, Hengrong Ni for assisting in the video shooting, and Rhea Chopra for the proofreading. We thank the National Science Foundation Grants (Career IIS2047912 and IIS2017008) for supporting this work.

REFERENCES

- [1] Leonard M Adleman. 1994. Molecular computation of solutions to combinatorial problems. *science* 266, 5187 (1994), 1021–1024.
- [2] Shiva Akhtarian, Hadi Veladi, Iraj Ahadzadeh, and Pouya Rezaei. 2021. Microfluidic Fredkin gate: A novel control unit for integrated microfluidic systems. *Microelectronic Engineering* 249 (2021), 111612.
- [3] Vannevar Bush. 1931. The differential analyzer. A new machine for solving differential equations. *Journal of the Franklin Institute* 212, 4 (1931), 447–488.
- [4] William A. S Buxton and Ronald M Baecker. 1987. *Readings in human-computer interaction: a multidisciplinary approach / written and edited by Ronald M. Baecker and William A.S. Buxton*. Morgan Kaufmann, Los Altos, Calif.
- [5] Stuart K. Card, Jock D. Mackinlay, and George G. Robertson. 1990. The Design Space of Input Devices. In *Proceedings of the SIGCHI Conference on Human Factors in Computing Systems* (Seattle, Washington, USA) (CHI '90). Association for Computing Machinery, New York, NY, USA, 117–124.
- [6] Yu-Wen Chen, Wei-Ju Lin, Yi Chen, and Lung-Pan Cheng. 2021. PneuSeries: 3D Shape Forming with Modularized Serial-Connected Inflatables. In *The 34th Annual ACM Symposium on User Interface Software and Technology* (Virtual Event, USA) (UIST '21). Association for Computing Machinery, New York, NY, USA, 431–440.
- [7] Rachel R Collino, Neil Reilly-Shapiro, Bryant Foresman, Kerui Xu, Marcel Utz, James P Landers, and Matthew R Begley. 2013. Flow switching in microfluidic networks using passive features and frequency tuning. *Lab on a Chip* 13, 18 (2013), 3668–3674.
- [8] Colter J Decker, Haihui Joy Jiang, Markus P Nemitz, Samuel E Root, Anoop Rajappan, Jonathan T Alvarez, Jovanna Tracz, Lukas Wille, Daniel J Preston, and George M Whitesides. 2022. Programmable soft valves for digital and analog control. *Proceedings of the National Academy of Sciences* 119, 40 (2022), e2205922119.
- [9] Alexandra Delazio, Ken Nakagaki, Roberta L Klatzky, Scott E Hudson, Jill Fain Lehman, and Alanson P Sample. 2018. Force jacket: Pneumatically-actuated jacket for embodied haptic experiences. In *Proceedings of the 2018 CHI conference on human factors in computing systems* (Montreal QC, Canada) (CHI '18). Association for Computing Machinery, New York, NY, USA, 1–12.
- [10] Jialin Deng, Patrick Olivier, Josh Andres, Kirsten Ellis, Ryan Wee, and Florian Floyd Mueller. 2022. Logic Bonbon: Exploring Food as Computational Artifact. In *CHI Conference on Human Factors in Computing Systems* (New Orleans, LA, USA) (CHI '22). Association for Computing Machinery, New York, NY, USA, 1–21.
- [11] Naga Sai Gopi K Devaraju and Marc A Unger. 2012. Pressure driven digital logic in PDMS based microfluidic devices fabricated by multilayer soft lithography. *Lab on a Chip* 12, 22 (2012), 4809–4815.
- [12] Dylan Drotman, Saurabh Jadhav, David Sharp, Christian Chan, and Michael T. Tolley. 2021. Electronics-free pneumatic circuits for controlling soft-legged robots. *Science Robotics* 6, 51 (2021), eaay2627.
- [13] Philip N Duncan, Transon V Nguyen, and Elliot E Hui. 2013. Pneumatic oscillator circuits for timing and control of integrated microfluidics. *Proceedings of the National Academy of Sciences* 110, 45 (2013), 18104–18109.
- [14] ECAL and MIT. Accessed: 2022-12-0. *ECAL - MIT Soft Machines*. ECAL/University of Art and Design Lausanne. <https://vimeo.com/371845881>
- [15] Sean Follmer, Daniel Leithinger, Alex Olwal, Nadia Cheng, and Hiroshi Ishii. 2012. Jamming user interfaces: programmable particle stiffness and sensing for malleable and shape-changing devices. In *Proceedings of the 25th annual ACM symposium on User interface software and technology*. Association for Computing Machinery, New York, NY, USA, 519–528.
- [16] Philipp Frank, David Gräfe, Christopher Probst, Sebastian Haefner, Martin Elstner, Dietmar Appelhans, Dietrich Kohlheyer, Brigitte Voit, and Andreas Richter. 2017. Autonomous Integrated Microfluidic Circuits for Chip-Level Flow Control Utilizing Chemofluidic Transistors. *Advanced functional materials* 27, 30 (2017), 1700430.
- [17] Tony Freeth, Yanis Bitsakis, Xenophon Moussas, John H Seiradakis, Agamemnon Tselikas, Helen Mangou, Mary Zafeiropoulou, Roger Hadland, David Bate, Andrew Ramsey, et al. 2006. Decoding the ancient Greek astronomical calculator known as the Antikythera Mechanism. *Nature* 444, 7119 (2006), 587–591.
- [18] Juri Fujii, Satoshi Nakamaru, and Yasuaki Kakehi. 2021. Layerpump: Rapid prototyping of functional 3d objects with built-in electrohydrodynamics pumps based on layered plates. In *Proceedings of the Fifteenth International Conference on Tangible, Embedded, and Embodied Interaction* (Salzburg, Austria) (TEI '21). Association for Computing Machinery, New York, NY, USA, 1–7.
- [19] Elizabeth Gallardo Hevia, Connor M McCann, Michael Bell, Nak-seung Patrick Hyun, Carmel Majidi, Katia Bertoldi, and Robert J Wood. 2022. High-Gain Microfluidic Amplifiers: The Bridge between Microfluidic Controllers and Fluidic Soft Actuators. *Advanced Intelligent Systems* 4, 10 (2022), 2200122.
- [20] Teng Han, Fraser Anderson, Pourang Irani, and Tovi Grossman. 2018. Hydroring: Supporting mixed reality haptics using liquid flow. In *Proceedings of the 31st Annual ACM Symposium on User Interface Software and Technology* (Berlin, Germany) (UIST '18). Association for Computing Machinery, New York, NY, USA, 913–925.
- [21] Yusuke Hara and Ryo Yoshida. 2008. Self-oscillating polymer fueled by organic acid. *The Journal of Physical Chemistry B* 112, 29 (2008), 8427–8429.
- [22] Helmut Hauser, Auke J Jjspeert, Rudolf M Fuchsli, Rolf Pfeifer, and Wolfgang Maass. 2011. Towards a theoretical foundation for morphological computation with compliant bodies. *Biological cybernetics* 105, 5 (2011), 355–370.
- [23] Liang He, Gierad Laput, Eric Brockmeyer, and Jon E Froehlich. 2017. Squeeze-Pulse: Adding interactive input to fabricated objects using corrugated tubes and air pulses. In *Proceedings of the eleventh international conference on tangible, embedded, and embodied interaction* (Yokohama, Japan) (TEI '17). Association for Computing Machinery, New York, NY, USA, 341–350.
- [24] Joshua D Hubbard, Ruben Acevedo, Kristen M Edwards, Abdullah T Alsharhan, Ziteng Wen, Jennifer Landry, Kejin Wang, Saul Schaffer, and Ryan D Sochol. 2021. Fully 3D-printed soft robots with integrated fluidic circuitry. *Science Advances* 7, 29 (2021), eahe5257.
- [25] Alexandra Ion, Ludwig Wall, Robert Kovacs, and Patrick Baudisch. 2017. Digital mechanical metamaterials. In *Proceedings of the 2017 CHI Conference on Human Factors in Computing Systems* (Denver, Colorado, USA) (CHI '17). Association for Computing Machinery, New York, NY, USA, 977–988.
- [26] Savita V Kendre, Lauryn Whitesides, Tian Y Fan, Jovanna A Tracz, Gus T Teran, Thomas C Underwood, Mohammed E Sayed, Haihui J Jiang, Adam A Stokes, Daniel J Preston, et al. 2022. The Soft Compiler: A Web-Based Tool for the Design of Modular Pneumatic Circuits for Soft Robots. *IEEE Robotics and Automation Letters* 7, 3 (2022), 6060–6066.
- [27] Seoktae Kim, Hyunjung Kim, Boram Lee, Tek-Jin Nam, and Woohun Lee. 2008. Inflatable Mouse: Volume-Adjustable Mouse with Air-Pressure-Sensitive Input and Haptic Feedback. In *Proceedings of the SIGCHI Conference on Human Factors in Computing Systems* (Florence, Italy) (CHI '08). Association for Computing Machinery, New York, NY, USA, 211–224.

- [28] Won-Kyu Lee, Daniel J Preston, Markus P Nemitz, Amit Nagarkar, Arthur K MacKeith, Benjamin Gorissen, Nikolaos Vasios, Vanessa Sanchez, Katia Bertoldi, L Mahadevan, et al. 2022. A buckling-sheet ring oscillator for electronics-free, multilateral locomotion. *Science Robotics* 7, 63 (2022), eabg5812.
- [29] Daniel C Leslie, Christopher J Easley, Erkin Seker, James M Karlinsey, Marcel Utz, Matthew R Begley, and James P Landers. 2009. Frequency-specific flow control in microfluidic circuits with passive elastomeric features. *Nature Physics* 5, 3 (2009), 231–235.
- [30] Guan hong Liu, Haiqing Xu, Xianghua Ding, Mingyue Gao, Bowen Li, Fushen Ruan, and Haipeng Mi. 2022. "It Puts Life into My Creations": Understanding Fluid Fiber as a Media for Expressive Display. In *CHI Conference on Human Factors in Computing Systems* (New Orleans, LA, USA) (CHI '22). Association for Computing Machinery, New York, NY, USA, 1–15.
- [31] Jasmine Lu, Ziwei Liu, Jas Brooks, and Pedro Lopes. 2021. Chemical haptics: rendering haptic sensations via topical stimulants. In *The 34th Annual ACM Symposium on User Interface Software and Technology* (Virtual Event, USA) (UIST '21). Association for Computing Machinery, New York, NY, USA, 239–257.
- [32] Qiuyu Lu, Jifei Ou, João Wilbert, André Haben, Haipeng Mi, and Hiroshi Ishii. 2019. MilliMorph – Fluid-Driven Thin Film Shape-Change Materials for Interaction Design. In *Proceedings of the 32nd Annual ACM Symposium on User Interface Software and Technology* (New Orleans, LA, USA) (UIST '19). Association for Computing Machinery, New York, NY, USA, 663–672.
- [33] Yiyue Luo, Kui Wu, Andrew Spielberg, Michael Foshey, Daniela Rus, Tomás Palacios, and Wojciech Matusik. 2022. Digital Fabrication of Pneumatic Actuators with Integrated Sensing by Machine Knitting. In *CHI Conference on Human Factors in Computing Systems* (New Orleans, LA, USA) (CHI '22). Association for Computing Machinery, New York, NY, USA, 1–13.
- [34] Hila Mor, Tianyu Yu, Ken Nakagaki, Benjamin Harvey Miller, Yichen Jia, and Hiroshi Ishii. 2020. Venous Materials: Towards Interactive Fluidic Mechanisms. In *Proceedings of the 2020 CHI Conference on Human Factors in Computing Systems* (Honolulu, HI, USA) (CHI '20). Association for Computing Machinery, New York, NY, USA, 1–14.
- [35] Bobak Mosadegh, Tommaso Bersano-Begley, Joong Yull Park, Mark A Burns, and Shuichi Takayama. 2011. Next-generation integrated microfluidic circuits. *Lab on a Chip* 11, 17 (2011), 2813–2818.
- [36] Kazunori Ogawa, Tomohiro Ikeda, and Yuichi Kurita. 2018. Unplugged Powered Suit for Superhuman Tennis. In *2018 12th France-Japan and 10th Europe-Asia Congress on Mechatronics*. IEEE, IEEE, Tsu, Japan, 361–364. <https://doi.org/10.1109/MECATRONICS.2018.8495845>
- [37] Jifei Ou, Mélina Skouras, Nikolaos Vlavianos, Felix Heibeck, Chin-Yi Cheng, Jannik Peters, and Hiroshi Ishii. 2016. aeroMorph-heat-sealing inflatable shape-change materials for interaction design. In *Proceedings of the 29th Annual Symposium on User Interface Software and Technology* (Tokyo, Japan) (UIST '16). Association for Computing Machinery, New York, NY, USA, 121–132.
- [38] Francisco Antonio Perdigonés, Antonio Luque, and Jose M. Quero. 2014. Correspondence Between Electronics and Fluids in MEMS: Designing Microfluidic Systems Using Electronics. *IEEE Industrial Electronics Magazine* 8, 4 (2014), 6–17.
- [39] Reid H Phillips, Rahul Jain, Yoni Browning, Rachana Shah, Peter Kauffman, Doan Dinh, and Barry R Lutz. 2016. Flow control using audio tones in resonant microfluidic networks: towards cell-phone controlled lab-on-a-chip devices. *Lab on a Chip* 16, 17 (2016), 3260–3267.
- [40] Daniel J Preston, Haihui Joy Jiang, Vanessa Sanchez, Philipp Rothmund, Jeff Rawson, Markus P Nemitz, Won-Kyu Lee, Zhigang Suo, Conor J Walsh, and George M Whitesides. 2019. A soft ring oscillator. *Science Robotics* 4, 31 (2019), eaaw5496.
- [41] Daniel J. Preston, Philipp Rothmund, Haihui Joy Jiang, Markus P. Nemitz, Jeff Rawson, Zhigang Suo, and George M. Whitesides. 2019. Digital logic for soft devices. *Proceedings of the National Academy of Sciences* 116, 16 (2019), 7750–7759.
- [42] Anoop Rajappan, Barclay Jument, and Daniel J Preston. 2021. Pneumatic soft robots take a step toward autonomy. *Science Robotics* 6, 51 (2021), eabg6994.
- [43] Anoop Rajappan, Barclay Jument, Rachel A Shveda, Colter J Decker, Zhen Liu, Te Faye Yap, Vanessa Sanchez, and Daniel J Preston. 2022. Logic-enabled textiles. *Proceedings of the National Academy of Sciences* 119, 35 (2022), e2202118119.
- [44] Karl N. Reid. 1969. Fluidic Devices and Their Steady-State Characteristics. *SAE Transactions* 78 (1969), 1934–1942.
- [45] Minsoung Rhee and Mark A Burns. 2009. Microfluidic pneumatic logic circuits and digital pneumatic microprocessors for integrated microfluidic systems. *Lab on a Chip* 9, 21 (2009), 3131–3143.
- [46] Harpreet Sareen, Udayan Umapathi, Patrick Shin, Yasuaki Kakehi, Jifei Ou, Hiroshi Ishii, and Pattie Maes. 2017. Printflatables: printing human-scale, functional and dynamic inflatable objects. In *Proceedings of the 2017 CHI Conference on Human Factors in Computing Systems* (Denver, Colorado, USA) (CHI '17). Association for Computing Machinery, New York, NY, USA, 3669–3680.
- [47] Valkyrie Savage, Carlos Tejada, Mengyu Zhong, Raf Ramakers, Daniel Ashbrook, and Hyunyoung Kim. 2022. AirLogic: Embedding Pneumatic Computation and I/O in 3D Models to Fabricate Electronics-Free Interactive Objects. In *Proceedings of the 35th Annual ACM Symposium on User Interface Software and Technology* (Bend, OR, USA) (UIST '22). Association for Computing Machinery, New York, NY, USA, Article 9, 12 pages. <https://doi.org/10.1145/3526113.3545642>
- [48] Stephen D Senturia and Microsystem Design. 2001. Massachusetts.
- [49] Rachel A Shveda, Anoop Rajappan, Te Faye Yap, Zhen Liu, Marquise D Bell, Barclay Jument, Vanessa Sanchez, and Daniel J Preston. 2022. A wearable textile-based pneumatic energy harvesting system for assistive robotics. *Science advances* 8, 34 (2022), eabo2418.
- [50] Saya Suzunaga, Yuichi Itoh, Yuki Inoue, Kazuyuki Fujita, and Takao Onoye. 2020. Tuve: A shape-changeable display using fluids in a tube. In *Proceedings of the International Conference on Advanced Visual Interfaces* (Salerno, Italy) (AVI '20). Association for Computing Machinery, New York, NY, USA, 1–9.
- [51] Carlos E. Tejada, Raf Ramakers, Sebastian Boring, and Daniel Ashbrook. 2020. AirTouch: 3D-Printed Touch-Sensitive Objects Using Pneumatic Sensing. In *Proceedings of the 2020 CHI Conference on Human Factors in Computing Systems* (Honolulu, HI, USA) (CHI '20). Association for Computing Machinery, New York, NY, USA, 1–10.
- [52] Shan-Yuan Teng, Tzu-Sheng Kuo, Chi Wang, Chi-huan Chiang, Da-Yuan Huang, Liwei Chan, and Bing-Yu Chen. 2018. Pupp: Pop-up prop on palm for virtual reality. In *Proceedings of the 31st Annual ACM Symposium on User Interface Software and Technology* (Berlin, Germany) (UIST '18). Association for Computing Machinery, New York, NY, USA, 5–17.
- [53] Jeroen ter Schiphorst, Janire Saez, Dermot Diamond, Fernando Benito-Lopez, and Albertus P. H. J. Schenning. 2018. Light-responsive polymers for microfluidic applications. *Lab Chip* 18 (2018), 699–709. Issue 5.
- [54] Todd Thorsen, Sebastian J Maerkl, and Stephen R Quake. 2002. Microfluidic large-scale integration. *Science* 298, 5593 (2002), 580–584.
- [55] Marc A Unger, Hou-Pu Chou, Todd Thorsen, Axel Scherer, and Stephen R Quake. 2000. Monolithic microfabricated valves and pumps by multilayer soft lithography. *science* 288, 5463 (2000), 113–116.
- [56] Alistair Martin Waddell, Jeff Punch, Jason Stafford, and Nicholas Jeffers. 2015. On the hydrodynamic characterization of a passive shape memory alloy valve. *Applied Thermal Engineering* 75 (2015), 731–737.
- [57] James A Weaver, Jessica Melin, Don Stark, Stephen R Quake, and Mark A Horowitz. 2010. Static control logic for microfluidic devices using pressure-gain valves. *Nature Physics* 6, 3 (2010), 218–223.
- [58] Penelope Webb, Valentina Sumini, Amos Golan, and Hiroshi Ishii. 2019. Auto-inflatables: Chemical inflation for pop-up fabrication. In *Extended Abstracts of the 2019 CHI Conference on Human Factors in Computing Systems* (Glasgow, Scotland UK) (CHI EA '19). Association for Computing Machinery, New York, NY, USA, 1–6.
- [59] Michael Wehner, Ryan L Truby, Daniel J Fitzgerald, Bobak Mosadegh, George M Whitesides, Jennifer A Lewis, and Robert J Wood. 2016. An integrated design and fabrication strategy for entirely soft, autonomous robots. *nature* 536, 7617 (2016), 451–455.
- [60] Junichi Yamaoka, Ryuma Niiyama, and Yasuaki Kakehi. 2017. BlowFab: Rapid Prototyping for Rigid and Reusable Objects Using Inflation of Laser-Cut Surfaces. In *Proceedings of the 30th Annual ACM Symposium on User Interface Software and Technology* (Québec City, QC, Canada) (UIST '17). Association for Computing Machinery, New York, NY, USA, 461–469.
- [61] Junichi Yamaoka, Kazunori Nozawa, Shion Asada, Ryuma Niiyama, Yoshihiro Kawahara, and Yasuaki Kakehi. 2018. AccordionFab: Fabricating Inflatable 3D Objects by Laser Cutting and Welding Multi-Layered Sheets. In *The 31st Annual ACM Symposium on User Interface Software and Technology Adjunct Proceedings* (Berlin, Germany) (UIST '18 Adjunct). Association for Computing Machinery, New York, NY, USA, 160–162.
- [62] Lining Yao, Ryuma Niiyama, Jifei Ou, Sean Follmer, Clark Della Silva, and Hiroshi Ishii. 2013. PneuUI: pneumatically actuated soft composite materials for shape changing interfaces. In *Proceedings of the 26th annual ACM symposium on User interface software and Technology* (St. Andrews, Scotland, United Kingdom) (UIST '13). Association for Computing Machinery, New York, NY, USA, 13–22.
- [63] Hiromi Yasuda, Phillip R Buskohl, Andrew Gillman, Todd D Murphey, Susan Stepney, Richard A Vaia, and Jordan R Raney. 2021. Mechanical computing. *Nature* 598, 7879 (2021), 39–48.
- [64] Qiongd Zhang, Ming Zhang, Lyas Djeghlaf, Jeanne Bataille, Jean Gamby, Anne-Marie Haghiri-Gosnet, and Antoine Pallandre. 2017. Logic digital fluidic in miniaturized functional devices: Perspective to the next generation of microfluidic lab-on-chips. *Electrophoresis* 38, 7 (2017), 953–976.